Measurement of the longitudinal spin-dependent neutron-proton total cross-section difference $\Delta\sigma_L(np)$ between 500 and 800 MeV

M. Beddo,* G. Burleson, J. A. Faucett,† S. Gardiner, and G. Kyle
New Mexico State University, Las Cruces, New Mexico 88003

R. Garnett,† D. Grosnick, D. Hill, K. Johnson,† D. Lopiano, Y. Ohashi,‡ T. Shima,§ H. Spinka, R. Stanek, D. Underwood, and A. Yokosawa
Argonne National Laboratory, Argonne, Illinois 60439

G. Glass,‖ R. Kenefick, S. Nath,† and L. Northcliffe
Texas A & M University, College Station, Texas 77843

J. J. Jarmer and S. Penttilä
Los Alamos National Laboratory, Los Alamos, New Mexico 87545

R. Jeppesen
University of Montana, Missoula, Montana 59812

G. Tripard
Washington State University, Pullman, Washington 99164

M. Devereux¶
Earlham College, Richmond, Indiana 47374
and Los Alamos National Laboratory, Los Alamos, New Mexico 87545

P. Kroll
University of Wuppertal, Wuppertal, Germany
(Received 11 January 1994)

A measurement of $\Delta\sigma_L(np)$, the difference between neutron-proton total cross sections for pure longitudinal spin states, is described. Data were taken at LAMPF for five neutron beam kinetic energies: 484, 568, 634, 720, and 788 MeV. The statistical errors are in the range 0.64–1.35 mb. Various sources of systematic effects were investigated and are described. Overall systematic errors are estimated to be on the order of 0.5 mb and include an estimate for the uncertainty in the neutron beam polarization. The $\Delta\sigma_L$ results are consistent with previous results from PSI and Saclay. These data, when combined with other results and fitted to a Breit-Wigner curve, are consistent with an elastic $I=0$ resonance with mass 2214 ± 15 (stat) ± 6 (syst) MeV and width $75 \pm 21 \pm 12$ MeV. Because of a lack of $\Delta\sigma_T(np)$ data between 500 and 800 MeV, it is not possible to differentiate between a singlet or coupled-triplet partial wave being responsible.

PACS number(s): 13.75.Cs, 13.88.+e, 14.20.Dh, 14.20.Pt

I. INTRODUCTION

The nucleon-nucleon (NN) interaction has been the subject of extensive experimental and theoretical investigation since the discovery of the atomic nucleus early in the century. This work has led to a fairly useful understanding of the NN interaction at energies below pion production threshold (about 300 MeV), which is the region of "conventional" nuclear physics, where elastic scattering dominates. The data for both proton-proton (pp) and neutron-proton (np) scattering are fairly copious at these energies and are generally self-consistent. From a theoretical point of view, quantitative success has been achieved in describing this process in terms of potentials based on field-theoretic formalism involving meson exchange. Among these are the Paris [1], Bonn [2], and Argonne [3] potentials. A review of this work has been given by Machleidt [4]. Other theoretical studies include Skyrme [5,6] and quark [7,8] models. The current status of these models has been reviewed by Vinh Mau [9].

At energies up to about 1 GeV, where pion production and excitation of the $\Delta(1232)$ resonance are possible, the situation is not so well understood, however.

*Now at Argonne National Laboratory, Argonne, IL 60439.
†Now at Los Alamos National Laboratory, Los Alamos, New Mexico 87545.
‡Now at Institute of Physical and Chemical Research, Wako, Saitama 351-01, Japan.
§Now at Kyoto Academy of International Culture, Katashirakawa, Sakyo-ku, Kyoto, Japan.
‖Now at University of Texas at Austin, Austin, Texas 78712.
¶Now at 127 Eastgate, Los Alamos, New Mexico 87544.

To completely characterize the elastic NN interaction requires knowledge of five complex amplitudes in both the isospin-one (I=1) and isospin-zero (I=0) channels. While the former have been experimentally determined fairly well at these energies, until very recently the latter were poorly known above about 500 MeV [10–14]. The major reason for this is that measurements of np scattering are needed to investigate the I=0 channel, whereas the I=1 channel is determined from pp scattering. Experiments involving neutrons are considerably more difficult than those involving only protons because of the poorer quality of the beams and the difficulty associated with the detection of neutrons. Consequently, the amount of np data available has been considerably smaller and its quality poorer from both a statistical and systematic point of view. The theoretical description at these energies is more complicated since the onset of inelasticities introduces additional complexity in describing the interaction. Theoretical studies here have been based on extensions of work at lower energies, but these have not had the quantitative success that was achieved there. Many of these calculations are discussed in Ref. [4].

One feature of particular interest that has emerged from studies in the higher-energy range is the possibility of the existence of broad dibaryon resonances. It had been generally felt that the NN system had no resonances since both the pp and np unpolarized total cross sections exhibit no pronounced structure. The first evidence contrary to this lack of structure was the discovery by Auer *et al.* [15] of peaks and dips in the total cross-section difference $\Delta\sigma_L(pp)$ in pure longitudinal spin states. This, together with other evidence, suggested the existence of $^1D_2$ and $^3F_3$, and possibly other, resonances with large inelasticities, represented by counterclockwise looping of the phase shifts [10–14]. This type of behavior can also result from inelastic thresholds, however, so that it is possible that these structures are related to the onset of Δ production and do not represent resonances. These conflicting possibilities have led to a great deal of controversy. A discussion of the history of dibaryons has been given by Locher *et al.* [16] and the current experimental situation is summarized in some of the Particle Data Group tables [17]. One of the more recent pieces of evidence is from Shypit *et al.* [18], who claim to have ruled out broad dibaryons in these partial waves at these energies on the basis of an analysis of their data on $pp \to np\pi^+$ in terms of $pp \to N\Delta$. Some objections to their interpretations have been raised, however [19–23]. There is also a fair amount of evidence for the existence of narrow dibaryons with a wide range of masses and widths, but this is also inconclusive [17].

Because of the unresolved nature of this structure in the I=1 channel, it is also important to carry out similar studies in the I=0 channel. One important feature of the I=0 channel is that it does not include Δ production, so that a major complication in this energy region is removed. Note that both $NN \to NN^*$ and $NN \to \Delta\Delta$ can occur at higher energies in both channels, however.

There are other reasons for carrying out experimental measurements to determine the amplitudes of the I=0 channel. One of them is that the NN interaction is a fundamental one for the nucleus and should be understood. Another is related to the work on studies of spin dependence in nucleon-nucleus interactions, which is investigating in particular the Dirac character of nucleons in the nucleus [24]. Theoretical calculations involving these interactions generally employ NN amplitudes as inputs, so that the poor knowledge of the I=0 amplitudes above 500 MeV can cause difficulties in the interpretation of the results.

For an experimental determination of the elastic I=0 amplitudes, measurements of total cross sections and differences of spin-dependent total cross sections are important, as they are for the I=1 channel. Elastic differential cross sections and cross-section asymmetries are generally related to products or squares of amplitudes, whereas total cross sections are related to sums of amplitudes, evaluated at 0°. Without total cross-section information, there will generally be discrete ambiguities in model-independent amplitude analyses. Moreover, data at small angles, as found in total cross-section measurements, can give important constraints for the fits to angular distributions. The slopes of $\Delta\sigma_L$ data, for example, are related to the elastic longitudinal spin-dependent parameter C_{LL}. In addition, total cross-section measurements give direct information on inelasticities, which serve as important constraints in phase-shift analyses.

There are several published measurements of $\Delta\sigma_L(np)$. The first of these [25] was carried out at Argonne and covered the momentum range of 1.1–6.0 GeV/c, using a polarized proton beam incident onto a polarized deuteron target, so that the quantity directly measured was $\Delta\sigma_L(pd)$. Values of $\Delta\sigma_L(pn)$ were extracted from these data including the use of spin-dependent Glauber-type corrections. After the original publication, additional corrections were applied to the data, one by Grein *et al.* [26] and another by the Argonne group [27]. Because of the momentum spread of nucleons in the deuteron ($\approx \pm 60$ MeV/c), these results represented averages over a range of neutron energies. In the energy range up to 1 GeV, the values of $\Delta\sigma_L(np)$ did not show any pronounced structure; so when $\Delta\sigma_L(I{=}0)$ was extracted with $\Delta\sigma_L(I{=}0) = 2\Delta\sigma_L(pn) - \Delta\sigma_L(pp)$, the behavior of $\Delta\sigma_L(pp) = \Delta\sigma_L(I{=}1)$ resulted in mirrorlike structure in $\Delta\sigma_L(I{=}0)$ [25]. A dispersion-relation analysis of this structure [26] found evidence for an abnormal-parity dibaryon ($1^+, 3^+, \ldots$) of mass 2.25 GeV and width about 100 MeV with high inelasticity. However, this group also carried out an analysis of the I=1 channel, with results disagreeing somewhat with phase-shift analyses.

Measurements of $\Delta\sigma_L(np)$ have also been carried out with a polarized neutron beam and a polarized proton target (PPT), both at Saclay and at the Paul Scherrer Institute (PSI). The PSI measurements [28] covered the energy range 140–590 MeV, while the Saclay measurements [29,30] were in the range 312–1100 MeV. These seem to be consistent with each other and with the originally published Argonne results, but not with the Argonne data as corrected later [30].

These new results from PSI and Saclay show structure in $\Delta\sigma_L(I{=}0)$ that is different from what was initially seen in the Argonne data, however. A current phase-

shift analysis [11] indicates no such structure, which reflects the poor knowledge of the $I=0$ partial waves in this energy region. There is also some disagreement on the strength of the $I=0$ inelastic channels at these energies [11,12,31,32].

This paper describes a set of measurements of $\Delta\sigma_L(np)$ at energies between 500 and 800 MeV, using a polarized neutron beam with a PPT. The work was carried out at the Clinton P. Anderson Meson Physics Facility (LAMPF) of the Los Alamos National Laboratory, as part of a program of measurements of np scattering aimed at the determination of the $I=0$ NN amplitudes at energies up to 800 MeV. These measurements were also made in order to compare the values of $\Delta\sigma_L(np)$ obtained with a neutron beam to those derived from $\Delta\sigma_L(pd)$, to check the validity of the corrections used with these data, as well as to obtain data having a smaller momentum spread compared with the neutrons in the deuteron. Preliminary results have been published previously [33]. Details of the experimental setup are discussed in Sec. II, and the data analysis is discussed in Sec. III. The results and an interpretation of them are given in Sec. IV, and a summary is given in Sec. V. Additional details can be found in Ref. [34], which was based on this work.

II. EXPERIMENTAL METHOD

A. General description

The polarized neutron beam at LAMPF is produced by the charge exchange, and resulting polarization transfer, of a polarized proton beam in a liquid deuterium target (LDT). The polarized proton beam is produced as H^- and is accelerated simultaneously with the more intense unpolarized H^+ beam. After acceleration, the two beams are separated and sent to different experimental areas.

For this experiment, a portion of the polarized H^- beam (P^-) was selected by passing it through thin strippers to produce a polarized H^+ beam. This beam was then sent through magnets used to bend, steer, and focus it, and to orient the direction of its polarization in the longitudinal direction. It also passed through a polarimeter, intensity monitors, and wire chambers used to monitor the beam profile and position. Signals from the latter were used in a feedback system to stabilize the beam position at a location immediately before the LDT. Downstream of this target, all remaining charged particles in the beam were deflected with dipole magnets and sent to a beam dump. The forward-going neutral beam, which consisted principally of neutrons and gamma rays, passed through a long collimator, intensity monitors, spin-precession magnets, and a polarimeter, before striking a longitudinally polarized proton target.

The neutrons passing through the PPT were detected downstream by a hodoscope of thick scintillation counters arranged in four successive planes that gave transverse position information. The asymmetry of detected scattered events for beam and target parallel and antiparallel was found as a function of momentum transfer, as defined by the geometry of the hodoscope, and extrapolated to zero momentum transfer. From this extrapolated point and the PPT parameters, the quantity $\Delta\sigma_L(np)$ was calculated. A diagram of the experimental setup is shown in Fig. 1.

B. The beam

1. *The polarized neutron beam*

The polarized proton beam was produced with a Lamb-shift H^- ion source [35], which typically provided a polarization of ~70%, with a current of ~20 nA. For acceleration to the maximum energy of 800 MeV, the duty factor was typically about 9%, but at lower energies it was less, as a result of time sharing with the H^+ beam. The energies of the beam were determined from the accelerator parameters.

Figure 2 shows the layout of the beam line immediately upstream of the experiment. After acceleration, the H^- beam was bent by magnets and had electrons stripped off portions of it by passage through thin foils or wire mesh, producing polarized H^+ beams that could be sent to three beam lines including the one used for these measurements. The relative intensities of these beams was adjusted by the type of strippers used. Spin-rotation magnets located at various positions allowed the directions of the polarizations in the different beam lines to be adjusted independently.

The neutron beam was produced by passing the polarized proton beam through a 25.4-cm-long LDT and selecting neutral particles produced at 0°. The measured spectrum [36] of forward-going neutrons was characterized by a narrow peak with an energy just below that of the proton beam, resulting from the charge-exchange reaction $pd \rightarrow npp$, and a well-separated continuum, resulting from inelastic reactions. The integrated intensities of these two regions were found to be roughly equal.

The maximum spin transfer from the polarized protons to the neutrons was shown in previous measurements [37,38] to be in the longitudinal direction. Accordingly, the direction of polarization of the proton beam was rotated to be longitudinal just before the LDT. This was accomplished with a solenoid (LB-SO) that rotated the spin from its initial vertical, or normal (N), direction to a "sidewise" (S) direction, followed by subsequent precession to an almost longitudinal (L) direction by the horizontal bending magnets in the beam line. The resulting polarization of the neutrons in the charge-exchange peak was ≈50%.

A magnet located just after the LDT deflected charged beam particles into a beam dump. At the same time, however, this magnet precessed the neutron spin away from its original longitudinal direction. The original spin direction was restored (and could also be reversed) by means of two magnets LORRAINE and CASTOR located 6.7 m and 4.6 m upstream of the polarized target, respectively. These magnets have been used extensively and their spin-rotation properties have been analyzed [39] with consistent results, so that their effects on the neutron spins are understood. Between the LDT and the experimental area the neutron beam passed through a

collimator in a 3.7-m-thick steel wall. This collimator consisted of cylindrical lead and steel slugs with holes in them centered on their axes, located inside a row of steel "gun barrels" in the wall: there was a 2.74-m section with 2.54-cm holes, followed by a 0.91-m section with 1.90-cm holes. The beam-intensity monitor counters, magnets, PPT, and neutron counter array were surveyed to be centered on the collimator axis before the experimental runs.

Since γ rays were also present in the neutron beam, it was important to attenuate them. Studies of counting rates with various thicknesses of lead plugs inserted at the end of the collimator indicated two attenuation curves, a short one, as expected for γ rays, and a longer one, associated with the neutrons in the beam. The attenuation length for the latter was about 9.5 cm. For data taking, a 2.54-cm plug (4.5 radiation lengths) was used, which attenuated the neutrons by about 25% and reduced the γ-ray flux by about 97%. The fraction of the remaining beam corresponding to γ rays was estimated to be less than 1%.

In order to find the size of the beam at the PPT, the beam profile was measured near the target using a small scintillation counter, about 3-mm thick, which was larger than the beam spot. It was oriented edgewise in the beam and moved transversely to the beam in both horizontal (x) and vertical (y) directions. Background counts were measured and subtracted. The resulting beam profiles, found at low intensities where most of the data were taken, are shown in Fig. 3. The full widths at half maximum (FWHM's) were 3.8 ± 0.3 cm (3.5 ± 0.2 cm) in x (y) and the full widths at 1/10 maximum (FWM_{10}'s) were 4.6 ± 0.3 cm (4.6 ± 0.2 cm) in x (y). Measurements at higher intensities gave a FWHM ≈ 3.4 cm. These values were unaffected by the neutron spin precession magnets. These numbers give a beam profile somewhat smaller than that previously observed [36], which, when projected to the PPT position, corresponds to a FWHM ≈ 4.7 cm and a $\mathrm{FWM}_{10} \approx 6.2$ cm. It should be noted that a larger-diameter collimator was used for those measurements, however. For a Gaussian beam profile, these results would imply that less than 3% of the beam missed the PPT (4.7 cm diameter). The systematic error due to this was taken to be about half this number.

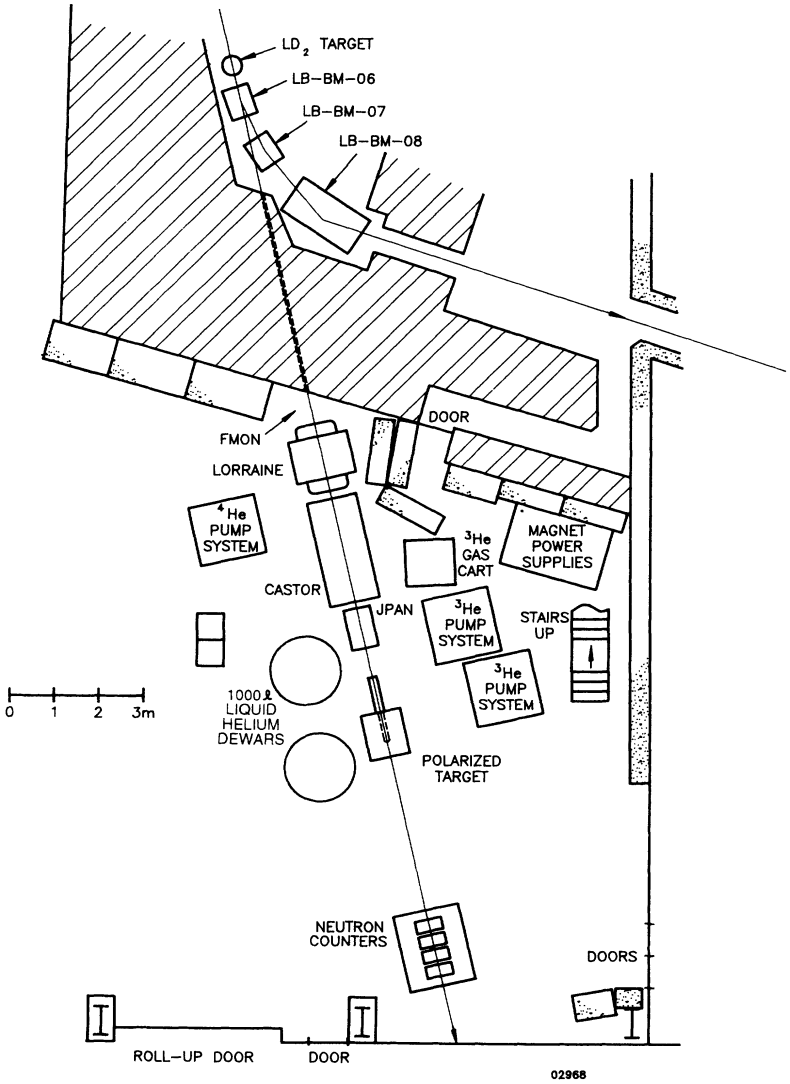

FIG. 1. Diagram of the experimental setup.

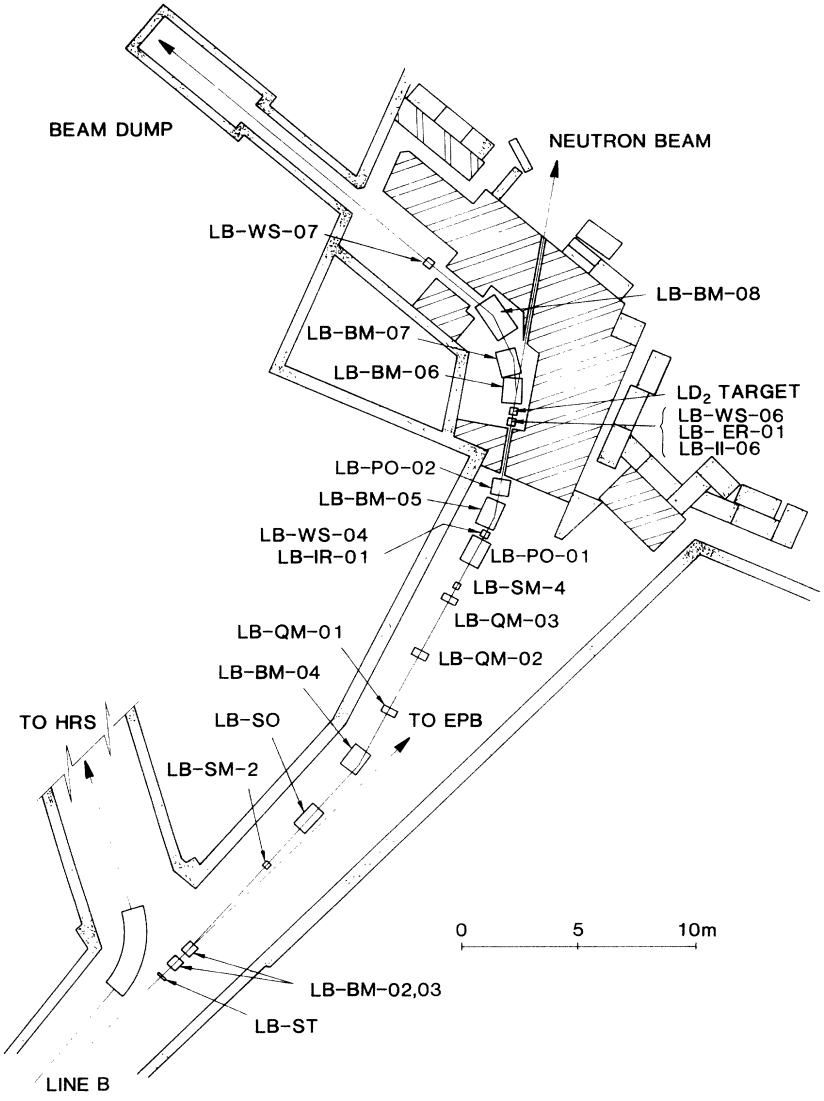

FIG. 2. Diagram of the experimental beam line.

2. Beam intensity measurements

The intensities of both the proton and neutron beams were monitored during this experiment (see also Sec. II B 4). Since the proton beam was considerably more intense than the neutron beam, the proton beam monitor was used to normalize the data and the neutron monitor was used as a check. The relative intensities of the two beams was kept fixed by a servo-steering mechanism described below.

The intensity of the proton beam was monitored with a secondary-emission monitor (SEM) that was located just upstream of the LDT. It consisted of one thin emitter foil located between two thin collector foils, enclosed in a vacuum. The emitter foil was maintained at a constant negative potential, typically −300 V, and the charge on the collectors was integrated by a charge digitizer [40], the output of which was a frequency proportional to the beam current. A relative measurement of the beam current was obtained by comparing this output with a reference clock.

The neutron beam intensity was monitored with a system of scintillation counters (FMON) located at the exit of the neutron collimator. A diagram of the system is shown in Fig. 4. The neutron beam first passed through a counter A, used to veto charged particles, and then through a block of polyethylene (CH_2), in which a small fraction of the beam interacted to give charged particles. After this were located another counter ($M1$), a pair of left-right counters ($M2$), a set of four counters defining quadrants ($M4$), a brass plate with a hole in its center, and a thick counter ($M3$) with a hole in its center. Various combinations of the signals from these counters were used to monitor both the intensity and the relative position of the neutron beam. A logical OR of the four $M4$ counters was used to give dead-time corrections for the data (see Secs. III A 3 and III B 2).

3. Beam polarization measurements

The principal means of monitoring the polarization of the proton beam was based on a particular type of op-

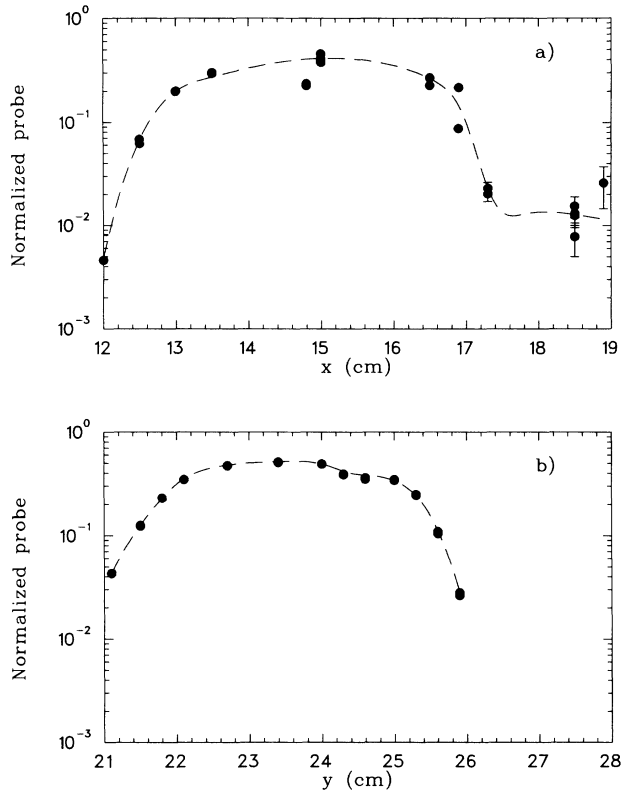

FIG. 3. Beam profile measured at 500 MeV. The abscissas represent the (a) horizontal or (b) vertical positions of the scintillator probe measured from an arbitrary origin. The FWHM was 3.8 ± 0.3 cm (3.5 ± 0.2 cm) in x (y). The curves are guides for the eye only.

eration of the polarized ion source. This source was of the Lamb-shift type, in which polarized H^- ions were produced in metastable states and selected to be accelerated [41]. In its normal or "run" operation, the beam exiting the source consisted of populations of polarized ions plus a small background of almost unpolarized ions. In the so-called "quench" mode of operation, the source was detuned so that the polarized ions were blocked, leaving only the almost unpolarized ions. A ratio of the ion currents in the normal and quenched mode gave an accurate measurement of the polarization of the beam. The typical mode of operation during the experiment was a sequence of two 60-s periods of "normal" and "reverse" spin directions, followed by a 10-s period of quench operation. This resulted in a measurement of the polarization of the beam every 130 s. The normal spin state is defined as that state for which the proton spins are oriented antiparallel to the beam momentum, at the LDT.

In addition, there were calibrated polarimeters, located in both the proton and neutron beams, that were used principally to set and monitor the directions of the polarization. Two polarimeters, separated by a bending magnet, were located in the proton beam, as shown in Fig. 2. The first LB-PO-01 was located just downstream of the last steering magnet and the second LB-PO-02 just upstream of the LDT. Each of these consisted of groups of counters used to detect the scattered and recoil protons from pp scattering in a CH_2 target block in the "left/right" and "up/down" directions. Any transverse polarization in the beam would produce an asymmetry in one or both of these sets of counters. The laboratory angle pair for these counters was 17° and 67°, chosen to give a maximum asymmetry over a region with minimum background and small sensitivity to angular variation. Details of these devices are given in Refs. [42,43].

A neutron polarimeter JPAN was located in the experimental area just downstream of the spin-precession magnets LORRAINE and CASTOR. A diagram of JPAN is shown in Fig. 5. It was used to determine the currents in these magnets to obtain the desired spin direction of the neutron beam and it was removed during data taking. JPAN consisted of a CH_2 target, followed by a scintillation counter ($N1$) used to detect charged particles produced in the CH_2, and four counters (NU, ND, NL, NR) located at 30° with respect to the beam to detect scattering in the up, down, left, and right directions. As with the proton beam, asymmetries in the up/down

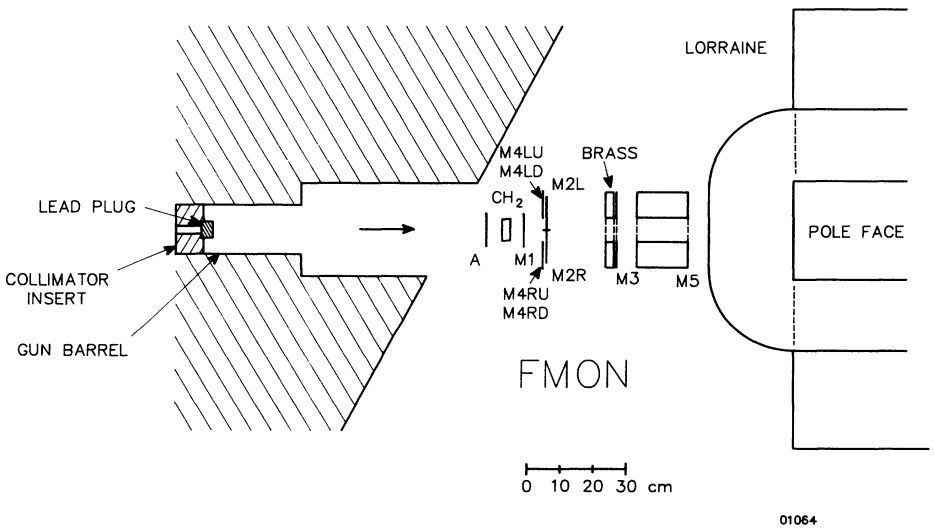

FIG. 4. Diagram of the neutron intensity monitor FMON. Details are given in the text.

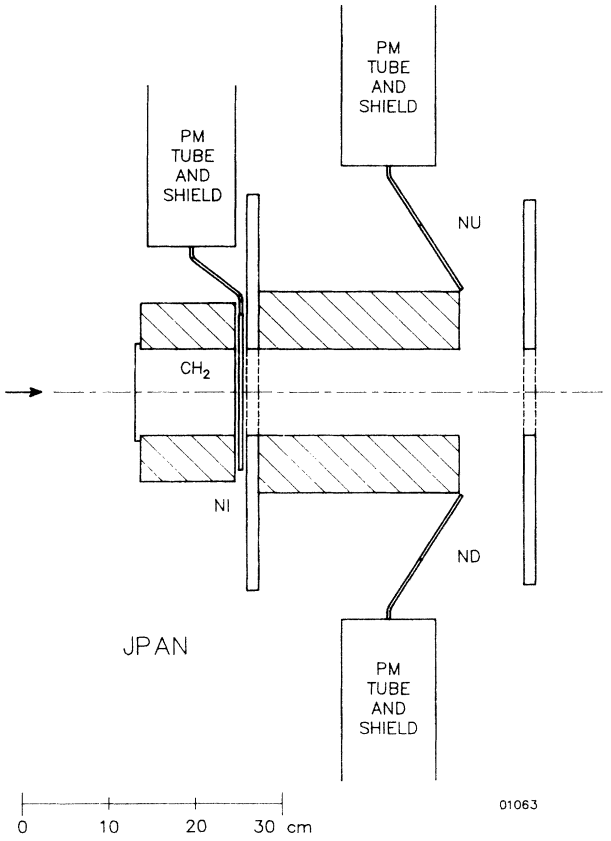

FIG. 5. Diagram of the neutron polarimeter JPAN. Details are given in the text.

of lower energy. With a 100-ns microstructure, however, this number would fall to nearly zero.

Accordingly, a bunching system was set up in the accelerator in order to produce a 100-ns microstructure in the P^- beam. The system consisted of two parts, located near the beam preaccelerator, which concentrated most of the beam current that was spread over 20 rf cycles into one rf cycle and chopped the small fraction of current that was not bunched. A more detailed description of this system is given in Ref. [34], which also describes a computer modeling of the system. The operation of the buncher was such that about 90% of the beam that was accelerated was bunched into one rf cycle, with a net reduction in average beam flux of about 40%.

An asymmetry in the fraction of the bunched beam that was within the time-of-flight window for the neutron detector array was measured. Since the principal beam intensity monitor, the SEM, was not sensitive to the time structure of the beam, it was necessary to correct for this in order to avoid a false asymmetry in the data. The measurements of this fraction were carried out with a charge-voltage-time analyzer module (QVT) [44] that was added to the system during the early stages of data aquisition. It recorded the time difference between the protons detected at LB-PO-01 and the 10-MHz reference signal of the buncher. The fraction f_{QVT} of the proton counts within the time-of-flight window was found for each beam spin change, and the SEM counts were multiplied by f_{QVT} to give the corrected monitor value. The asymmetry in f_{QVT} was typically 10^{-3}.

5. The beam steering system

A systematic motion of the LAMPF P^- beam with spin direction at the LDT had been observed. Since the principal monitor of the beam flux in this experiment was the SEM, located in the proton beam just upstream of the LDT, and since this target did not have flat end windows, such beam motion would lead to a varying path length through this target. This would therefore modify the neutron-to-proton beam flux ratio systematically and produce a false asymmetry. Experimental studies of the resulting neutron-to-proton flux ratio, as the beam spot position at the LDT was varied, showed that the systematic error on $\Delta\sigma_L$ could be as large as 30 mb for changes in the beam spot position of 1 mm. The magnitude of this error varies quadratically with the position changes. A good determination of $\Delta\sigma_L$ required asymmetry measurements at the level of $\pm 10^{-4}$, which in turn required that the beam position on the LDT be stable to ± 0.1 mm. In order to meet this need, a beam steering system based on feedback of beam position information was designed and implemented [45].

In the operation of this system, the transverse profiles of the beam in perpendicular planes were measured continuously with a beam profile monitor, similar to a multiwire proportional chamber, and it was located between the SEM and the LDT. These signals were read into a beam-line computer, which calculated the centroid and standard deviation of the beam profiles using several separate data buffers. This information was used to maintain the desired beam position by feedback to horizontal and vertical beam steering magnets. Each of the data buffers accumulated over a different time interval for various levels of control. Buffers with short time constants corrected large steering errors quickly, while those with longer time constants corrected increasingly smaller steering errors. In addition, separate buffers were used for normal and reverse spin states. Parameters of the system were adjusted to control the response time, which could give either too slow a response or oscillations if improperly chosen. The system was capable of reading a profile every beam macropulse (40 Hz) and could calculate centroids, standard deviations, and steering corrections in about 0.1 s. The optimum position of the beam was initially found by sweeping the proton beam across the LDT and maximizing the neutron-to-proton ratio, demonstrated in Fig. 6 for 800-MeV protons. The beam profile was established by the tune of the beam and was not adjusted by this system.

The computer software allowed continuous monitoring with this system. Overall, it was not difficult to maintain the beam position to the required precision (see Figs. 7–9). The only problems encountered were related to the occasional appearance of a long tail on one side of the beam profile due to the beam being mistuned or occasions when the beam-steering magnets reached the limits

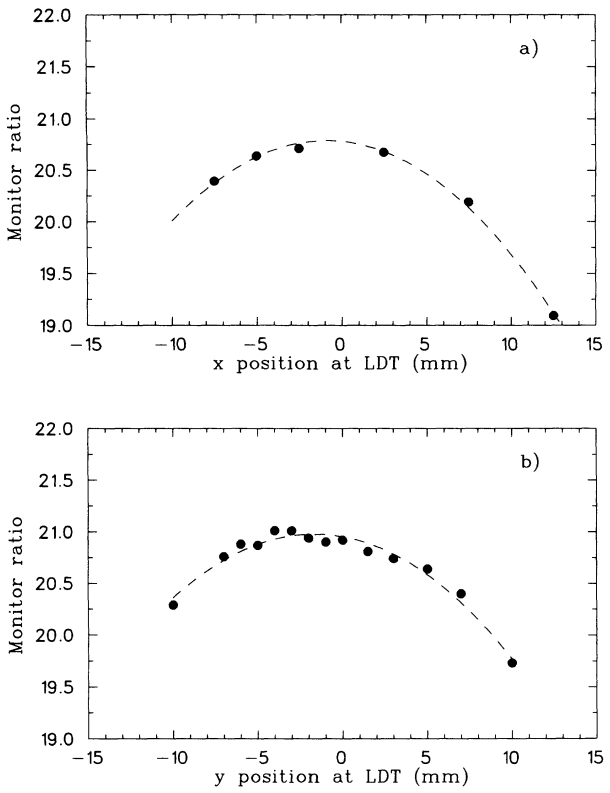

FIG. 6. Ratio of FMON counts to SEM counts (proportional to neutron/proton ratio) vs beam position at the liquid deuterium target (LDT). The abscissas are the beam spot positions at the LDT for the (a) horizontal or (b) vertical directions. The dashed lines are guides for the eye only. Using such data, the beam steering parameters were set.

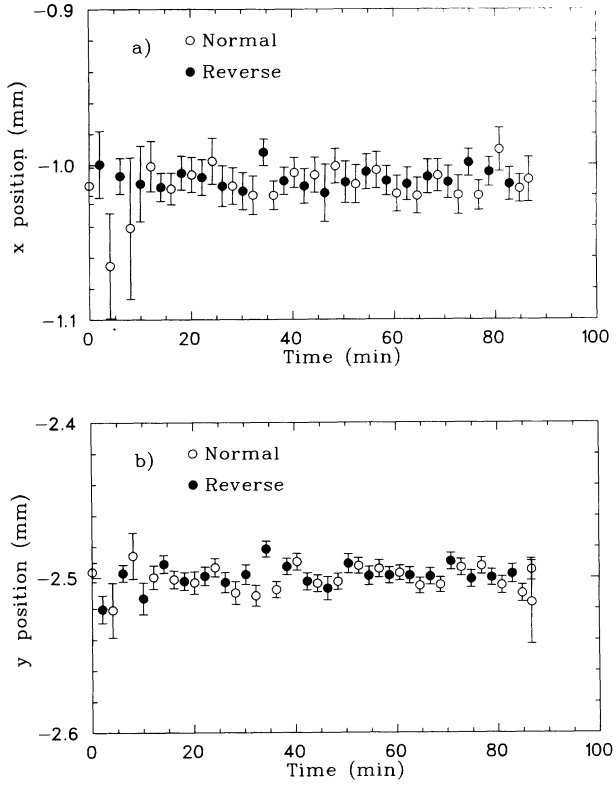

FIG. 7. Typical time history of the beam position at the LDT with the feedback steering system for proton beam spin states normal and reverse. The (a) x and (b) y positions were kept fixed to within ± 0.1 mm.

of their allowed range. In such cases, appropriate modifications were easily made.

C. The polarized target

Hydrogen nuclei in the PPT were polarized dynamically by using microwave spin pumping [46]. The longitudinally polarized proton target consisted of a horizontal ^{3}He-evaporation refrigerator operating near 0.5 K, a superconducting solenoid magnet with a horizontal warm bore, a large pump system to circulate ^{3}He gas, a microwave source, and a nuclear magnetic resonance (NMR) polarization monitor.

The PPT material was 1,2-propanediol doped with EHBA-Cr^V paramagnetic complex [47] to a level of 6×10^{19} spins/cm^3. The material was frozen in the form of ~1-mm-diam beads, which were contained in a thin-wall cylindrical holder made of FEP Teflon. The holder was perforated to allow free circulation of the ^{3}He, which was contained within a somewhat larger cylindrical vessel made of TFE Teflon. At room temperature, the holder was 4.75 ± 0.10 cm in diameter and 12.54 ± 0.08 cm in length, and was oriented with the cylinder axis along the beam. Microwave power at frequencies near 70 GHz was distributed along the PPT length by using a slotted waveguide. Reversals of the PPT polarization were accomplished by a small change of microwave frequency.

The iron-free, superconducting polarizing magnet [48] operated near 4.2 K and generated a solenoidal field of 2.5 T, which was uniform to 10^{-4} over the volume of the PPT. The magnetic field vector was in the direction of the beam momentum.

An existing horizontal ^{3}He-evaporation cryostat was modified to cool this relatively large target and also to provide a low-mass, axial, 5-cm-diam beam access to the target. A high-cooling capacity target insert was built and used with a 9600-m^3/h-displacement pumping system. The cooling capacity was 280 mW at 0.5 K, achieved with a ^{3}He circulation of ~7 mmol/s.

The PPT polarization was continuously monitored with a frequency-sweep NMR system using a PDP-11/23 microprocessor [49]. Three separate NMR coils were used to sample the proton polarization at different regions in the PPT. The scattering data for this experiment were taken during two LAMPF running periods that were separated in time by a few months, and the sampling region for one of the coils was changed between these different sets of runs. For the first set, all three coils were wrapped around the outer circumference of the target holder, two hairpin coils at each end and a saddle coil around the middle part. For the second set, the end coils remained the same, but the saddle coil was changed to a hairpin immersed in the beads along the PPT axis in order to

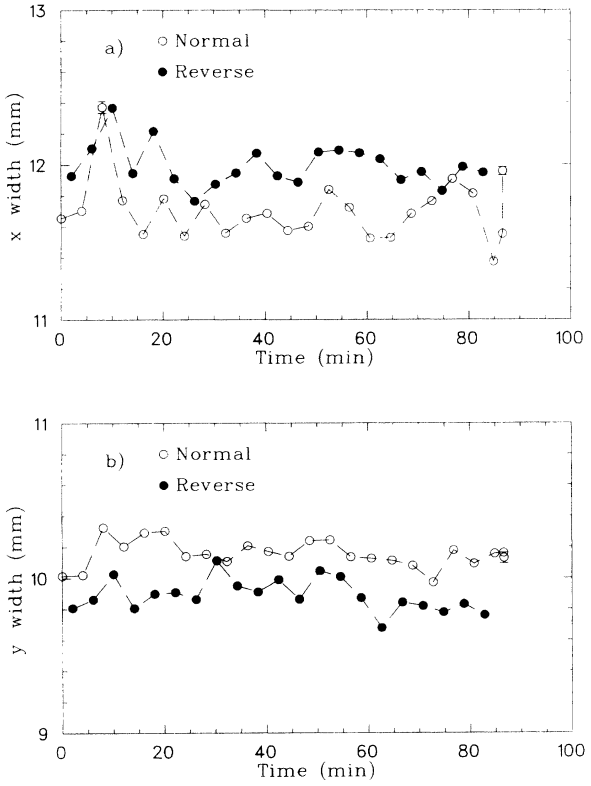

FIG. 8. Typical time history of the beam width (one σ) at the LDT. The dashed lines are guides for the eye only. Note systematic difference between normal and reverse spins.

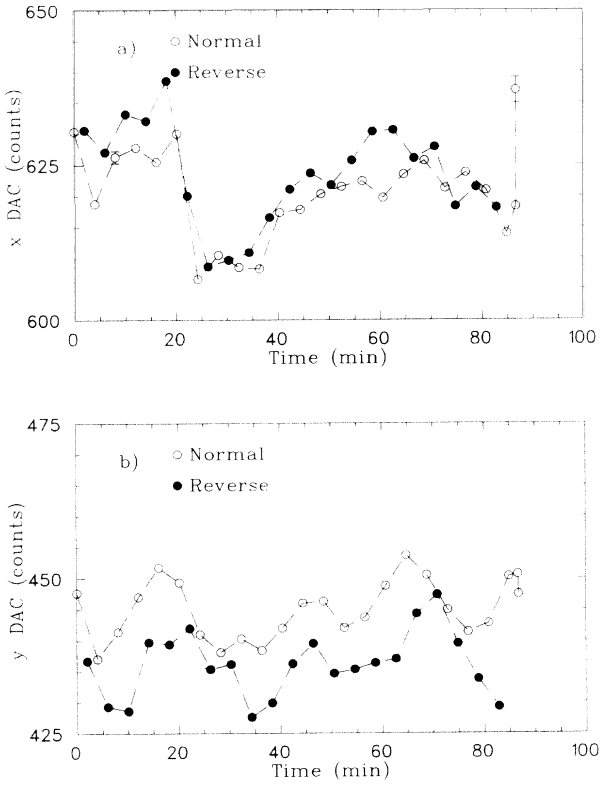

FIG. 9. Typical time history of the DAC (digital-to-analogue converter) signal, which is proportional to magnet current, for the beam steering magnets. The dashed lines are guides for the eye only. Note systematic difference in magnet currents required to maintain the beam position at the LDT for normal and reverse spins.

sample the target interior more effectively. The calibration of the NMR system was checked at approximately weekly intervals by measuring the thermal equilibrium signals at 1 K. The polarization direction was reversed at 6–8 h intervals.

The polarization achieved was typically 63% for PPT spin parallel to the magnetic field and 70% for the antiparallel case. This asymmetry is somewhat greater than is usually experienced and is attributed to the large size of this target relative to the cooling provisions. The polarizations have an estimated uncertainty of 6.2% of the measured values, mainly due to uncertainty about the spatial uniformity of the polarization within the target.

D. The neutron counter array

Neutrons passing through the PPT were detected downstream in an array of thick plastic scintillation counters that consisted of 24 counters arranged in planes of six counters each, with a charged-particle veto in front. The active volume of each counter was $11.4\times25.4\times61.0\,\mathrm{cm}^3$ of NE-102 plastic scintillator. Including the dimensions of the scintillator containers and cushioning, the total area of each counter plane was $76\times61\,\mathrm{cm}^2$ facing the beam. A 32-cm-long Lucite light guide was glued onto each end of the scintillator blocks and 12.7-cm-diam photomultiplier tubes were optically coupled to the light guides with optical grease [50]. The photomultipliers were offset 5 cm from the counter center along the beam direction to allow the counters to be close packed. The counters were oriented with the 25.4-cm dimension along the beam and adjacent planes of counters were oriented perpendicular to each other. More details of the arrangement are given in Refs. [34,51]. The full array could be rotated through 360° and moved horizontally, vertically, or along the beam direction.

Two independent methods were used to determine the interaction point of a neutron in the counter array. The first method used the information from coincidences between counters in adjacent planes to localize the event. The second method used fast time-to-digital converters (FTDC's) [52]. These determined the interaction point in a counter from the time difference between the signals from the photomultipliers on the two ends. Each of these two methods defined the interaction points in a square grid pattern formed by the counters.

In order to reject most low-energy neutrons in the beam, cuts were made on the time of flight from the LDT to the neutron counter array. By using the neutron beam, signals from each neutron counter were individually delayed so that they were all synchronized to within ±0.5 ns. A logical *OR* of these signals was formed and its timing relative to the 10-MHz buncher signal was determined with a FTDC. The position of the sharp

peak corresponding to the desired neutrons in the beam was continuously monitored with scalers. Overall timing drifts of a few nanoseconds were often observed and corrected. Some causes of these drifts were changes in the accelerator operating conditions needed by other experiments and temperature changes of propagation velocity in long cables carrying the 10-MHz signal to the experiment. The FTDC output, corresponding to a timing window of 2.2 ns, was used as a requirement for the desired events in the electronic logic.

The gains of the counters were set, and monitored during data taking, with cosmic-ray signals in order to ensure that there were no sudden changes. If cosmic-ray events, which were mostly minimum-ionizing muons, were selected with electronic logic that required a coincidence in three adjacent counters in a plane, the resulting photomultiplier pulse-height spectra showed clear peaks. The positions of these peaks indicated the relative gains of the counters. Since the angular distribution of cosmic rays is strongly peaked in the vertical direction, the peaks seen in counters oriented vertically were greater in pulse height (by a factor of 1.25–1.4) and broader than in counters oriented horizontally, due to longer path lengths. This behavior was computer modeled [34,51], with results that were in satisfactory agreement with what was observed both in peak shape and relative pulse heights. This calculation also predicted that the cosmic-ray rates in the horizontal counters should be greater than those in the vertical counters by a factor of about 3, compared with the experimental value of 3.4. The gains of the photomultiplier tubes were reasonably stable over long periods of time, with variations $\lesssim 5\%$ over periods of several weeks.

A measurement [51] of the detection efficiency of these counter arrays was performed for neutrons of energies 289 and 435 MeV. The PPT was replaced with a liquid hydrogen target and the neutrons that were elastically scattered from this target were detected in coincidence with the recoil protons, which were detected in a range telescope of scintillation counters and identified with time-of-flight methods and by their range in the scintillators. The results indicate that the total neutron detection efficiency at these energies for three layers of the array was nearly 50%. The detailed results were compared with a simulation using the Monte Carlo neutron detection program of Sailor *et al.* [53], which predicted values 5–15 % higher than the measured efficiencies. Knowledge of the absolute detection efficiency was not necessary for the determination of $\Delta\sigma_L$.

III. DATA ANALYSIS

A. The experimental trigger logic

1. General description

The data for this experiment were collected entirely from scaler information, as opposed to event by event recording. As mentioned above, the interaction points of neutrons in the detector array were determined by two methods. In the first method coincidences between signals from counters in each plane that registered a hit were recorded. The interaction point of an event was taken to be the square area defined by the geometrical intersection of the profiles of counters in adjacent planes. In the second method, the time difference between signals from the photomultiplier tubes on the two ends of each counter were sent to FTDC modules, for each event. The outputs of these modules corresponded to various values of these time differences, which in turn corresponded to different regions along the length of the counters. The spatial resolution given by this method was similar to that of the coincidence method. Because the first method required an interaction to give a signal in two adjacent planes, whereas the second method required a signal in only one plane, the number of events recorded using the second method was greater. Values of $\Delta\sigma_L(np)$ determined by the two methods were consistent, but the final results reported here are based on the time-difference method since the statistical errors are smaller.

The data aquisition system consisted of a computer and CAMAC modules read via a microprogrammable branch driver [54]. This computer also was used to monitor the quality of the beam bunching, the steering of the beam at the LDT, the beam intensities as indicated by the beam monitors, the beam polarization as indicated by the quench method and by the beam polarimeters, and the PPT polarization. As noted above, the gains of the neutron counters were measured during data taking with cosmic-ray events, which were gated between beam pulses.

Scaler information was recorded for each beam spill. During the data taking, various scaler ratios and beam spin direction asymmetries were calculated in either a differential form, for specified time intervals, or an integral form. The most important of these ratios were those corresponding to possible beam instabilities, such as the proton and neutron beam intensities, the time-of-flight operation, and the beam buncher and/or chopper operation. The computer also calculated quantities proportional to $\Delta\sigma_L$ for each successive pair of beam spin directions.

2. The coincidence logic

Since there was a total of four planes of six counters per plane, the intersection of counters in adjacent planes divided the xy planes (perpendicular to the beam direction) into sets of 36 bins at three different z positions (located between adjacent planes along the beam direction). The nominal area of a bin was $12.7 \times 12.7\,\mathrm{cm}^2$. Only 24 of the bins were used in the analysis, however, since the acceptance of the outermost bins was limited by the size of the counters. Both real and accidental coincidences were scaled, so a total of 216 scaler channels were needed.

The logic system used with this method is detailed in Refs. [34,51]. The inputs were the time-averaged coincidences between signals from the photomultiplier tubes on the ends of each neutron counter. The appropriate coin-

cidences, and the corresponding accidental coincidences, which were of the order of 1% of the signal, were formed with a set of strobed-coincidence modules, all gated with the neutron time-of-flight signal. This rate was not dependent on beam spin direction.

3. The FTDC logic

The LAMPF accelerator timing is based on a 201.25-MHz reference frequency. With the beam chopper operation, a stable 10-MHz timing signal was used as a reference. The second method used the time difference between photomultiplier signals from the two ends of each neutron counter. This difference was found with the FTDC's and, together with the time-of-flight gate, gave position information for neutrons near the beam energy interacting in each counter. Each FTDC had eight output channels, two of which represented underflows and overflows, so that six channels were available for position information. The bin widths for the time differences were 1.25 ns, which corresponded to bin widths in position of ~10 cm. This was checked by moving the counters laterally in a beam. A dead time of 250 ns was required for the FTDC's to reset after digitizing a signal, so the system was gated off during this time. The logic was set so that a plane of counters having a signal vetoed signals of planes farther downstream. Three of the four planes were instrumented with this logic.

B. The analysis of the data

1. Filtering the data

Scaler data were recorded on tape on a spill-by-spill basis, so that systematic effects could be studied and reduced. For each run, ratios of scalers representing various pieces of information were calculated and studied for possible systematic variations. These included the proton beam monitors, the neutron-to-proton beam ratio, the fraction of the beam within the time-of-flight window, and the buncher and/or chopper fraction. A statistical method based on Chauvenet's criterion [55] was used to reject portions of the data. Less than 10% of the data were rejected in this manner. In some cases, systematic effects were clearly present, or many spills were found to have large variations from the mean, so that such portions of the runs were rejected, or occasionally the entire run was rejected.

2. The calculation of $\Delta\sigma_L$

The number of neutrons detected in each geometrical bin in the neutron counter array was normalized to the proton beam monitor (SEM), which was corrected for dead time as measured in the neutron beam monitor system (FMON), which was gated to give the ratio of live time to total time. For the coincidence method, corrections were made for accidental counts, which in all cases amounted to only a few percent. Accidental counts in the FTDC method were corrected for as indicated in Sec. III B 3. If $T^{\pm}$ represents the normalized numbers of neutrons detected in a bin for spins parallel (+) and antiparallel (−), an asymmetry ϵ was calculated using

$$\epsilon = \frac{T^+ - T^-}{T^+ + T^-} , \tag{1}$$

with a statistical uncertainty given by

$$\delta\epsilon = \frac{\left[(\delta T^+)^2(1-\epsilon)^2 + (\delta T^-)^2(1+\epsilon)^2\right]^{1/2}}{T^+ + T^-} . \tag{2}$$

The errors $\delta T^{\pm}$ contain the errors on the numbers of detected neutrons, taken to follow a Poisson distribution, and the errors on the beam dead time, taken to follow a binomial distribution. The uncertainties in the beam monitor (SEM) were not included in the statistical error calculation since they stemmed from a systematic effect. This uncertainty corresponded to a dark current that was present even in the absence of beam and it was estimated from the counts in the SEM digitizer as found in the run and quench modes of beam operation. This is discussed further below.

Each geometrical bin corresponded to a different momentum transfer t, where $t = (p_1 - p_3)^2$, and p_1 and p_3 are the four-momenta for the incident and elastically scattered neutrons, respectively. The value of t corresponding to a bin was taken to be the unweighted value for that bin, given by

$$\langle t \rangle = \frac{1}{s}\int t\, ds , \tag{3}$$

where s is the total area of the bin. The linear extrapolation of ϵ to $\langle t \rangle = 0$ was found to be insensitive to how $\langle t \rangle$ was defined.

For small ϵ, the total cross-section difference $\Delta\sigma_L(np)$ is related to the extrapolated asymmetry $\epsilon(0)$ by

$$\begin{aligned}\Delta\sigma_L &\equiv \sigma^{\mathrm{tot}}(-) - \sigma^{\mathrm{tot}}(+) \\ &= \frac{2A}{P_n P_p}\epsilon(0) ,\end{aligned} \tag{4}$$

where P_n and P_p are the neutron beam and PPT polarizations, and A is the target constant. If the target beads are uniformly distributed within the target holder, and letting a be the cross-sectional area of the holder and N_{H} the total number of hydrogen nuclei in the target, then

$$\begin{aligned}A = \frac{a}{N_{\mathrm{H}}} &= \frac{\pi D^2 M_{\mathrm{H}}}{4fMN_A} \\ &= \frac{1315D^2}{fM} ,\end{aligned} \tag{5}$$

where N_A is Avogadro's number, M_{H} the atomic mass of hydrogen, D the diameter of the holder, M the total mass of the target, and f is the weight fraction of hydrogen in the target material.

The target beads were loaded into the target holder at liquid nitrogen temperature; therefore, the warm holder

diameter given in Sec. II C must be corrected for the thermal shrinkage of 1.7% for FEP Teflon. Allowing for some uncertainty in the shrinkage factor, one has $D = 4.67 \pm 0.12$ cm. Two different batches of beads were used during the two running periods and chemical analyses were performed on each. For the first target, the measured value of f was 0.0995, and for the second, 0.1063. There is no reason to believe that the two batches were actually of significantly different composition nor that either should have departed significantly from the weight fraction (0.1043) as estimated from the nominal chemical composition of the target material. The calculation for A therefore uses the value corresponding to the nominal composition and assign an uncertainty equal to one-half of the difference between the analytical results: $f = 0.1043 \pm 0.0034$. At the end of both periods, the target material was recovered and weighed. For the first target, the measured mass was 154.2 ± 0.1 g, and for the second, 137.2 ± 1.4 g. The target holder volume was essentially the same for the two periods. (The NMR coil that was inserted in the holder for the second period occupied negligible volume, $<1\,\mathrm{cm}^3$.) Since the mass of the first target was close to that expected for a well-packed target, it must be assumed that the second target had voids in the bead packing. For the first target, the target constant [Eq. (5)] is

$$A = \frac{1315(4.67 \pm 0.12)^2}{(0.1043 \pm 0.0034)(154.2 \pm 0.1)} = 1780 \pm 110\,\mathrm{mb}\,. \quad (6)$$

Since any voids in the second target would be expected to be predominately at the top of the target where the beam profile was relatively small, this same value for A has been used for the second period, but the estimated uncertainty has been expanded by half of the difference between target masses: $A = 1780 \pm 150$ mb.

The neutron beam polarization P_n was obtained using the proton beam polarization components and the spin transfer functions K_{LL} and K_{NN}. If P_{LDT} and θ_{LDT} are the proton polarization and spin direction at the LDT, respectively, then the neutron polarization magnitude is

$$|P_n| = K_{\mathrm{eff}}|P_{\mathrm{LDT}}|,$$
$$K_{\mathrm{eff}} = \left[(K_{LL}\cos\theta_{\mathrm{LDT}})^2 + (K_{NN}\sin\theta_{\mathrm{LDT}})^2\right]^{1/2}. \quad (7)$$

Recently, measurements at LAMPF [56] of the longitudinal spin transfer in the $d(\mathbf{p},\mathbf{n})X$ reaction at 300, 484, 634, 720, and 788 MeV found values of K_{LL} that are about 15% larger than those previously published [37,38]. Values for the spin transfer functions have been adopted that are essentially weighted averages of the results of Refs. [38,56]. An extensive analysis of this question will be presented in a forthcoming paper [57]. Table I lists the values for the K functions used in the present analysis, as well as K_{eff}, for each energy.

TABLE I. Spin directions for the protons at the LDT, spin transfer functions K_{LL} and K_{NN}, and the corresponding derived effective spin transfer K_{eff} as a function of energy (see text). The pairs of angles listed correspond to the proton spin directions during the normal and reverse spin states, respectively. The coordinate system defining θ_{LDT} is given in Ref. [39], with the $+L$-type spin corresponding to 0° and the $+S$-type spin to 90°. The magnitude of the polarization of the neutron beam is K_{eff} times the polarization of the proton beam.

T_{lab}	θ_{LDT} (degrees)				
(MeV)	Normal	Reverse	K_{LL}	K_{NN}	K_{eff}
484	182.0	+2.0	−0.580	−0.186	0.580
568	177.0	−3.0	−0.643	−0.135	0.642
634	173.0	−7.0	−0.691	−0.086	0.686
720	167.8	−12.2	−0.717	−0.090	0.701
788	163.6	−16.4	−0.713	−0.092	0.684

3. *Correlation studies*

In order to reduce any residual systematic effects, correlations between the extrapolated asymmetry $\epsilon(0)$ and various experimental parameters were studied for a large number of runs at each energy. For this work, a modification of the relation between $\epsilon(0)$ and $\Delta\sigma_L$ given in Eq. (4) was used:

$$\epsilon(0) = \frac{P_n P_p}{2A}\Delta\sigma_L + \alpha\epsilon_{\mathrm{QVT}} + \beta\frac{T}{C_{\mathrm{SEM}}}\epsilon_{T/C_{\mathrm{SEM}}} + \gamma\frac{C_{\mathrm{acc}}}{N}\epsilon_{C_{\mathrm{acc}}/N} + \delta\,, \quad (8)$$

where α, β, γ, δ, and $(\Delta\sigma_L/2A)$ were the fitted parameters. The quantity ϵ_{QVT} was related to the fractions $f^{\pm}_{\mathrm{QVT}}$ of the beam bunched within a single rf cycle for beam spins normal and reverse, so that ϵ_{QVT} was given by

$$\epsilon_{\mathrm{QVT}} = \frac{f^{+}_{\mathrm{QVT}} - f^{-}_{\mathrm{QVT}}}{f^{+}_{\mathrm{QVT}} + f^{-}_{\mathrm{QVT}}}\,. \quad (9)$$

Values of f_{QVT} were typically 90–95 %. The quantity T/C_{SEM} and its associated asymmetry $\epsilon_{T/C_{\mathrm{SEM}}}$, defined analogously to the above, is the ratio between the counts from the SEM proton beam monitor and the time duration of a data run T. It was used to account for both the beam-independent dark current in the SEM and the cosmic rays detected in the neutron counters during data taking, both of which were related to the fraction of time the beam was on during a run. The quantity C_{acc}/N and its associated asymmetry $\epsilon_{C_{\mathrm{acc}}/N}$ were used with the time-of-flight logic to account for accidental counts, which were not corrected for but should be proportional to the ratio of accidentals to beam neutrons (C_{acc}/N) as seen in the coincidence logic. The quantity δ represents a constant offset term that was found necessary to give good χ^2 values to some of the fits and represents an unknown systematic effect (see below).

Data from the FTDC logic and the coincidence logic were fitted separately to Eq. (8), grouped according to energy. Data sets corresponding to separate planes in the detector array (or pairs of planes for the coincidence logic) were treated separately. Whenever one of the fit-

ted parameters was found to be consistent with zero, the terms corresponding to that correlation were removed from the fit.

Results of these fits are given in Table II, which includes values of the reduced χ^2 for each case. In addition to $\Delta\sigma_L$, the only fitted parameter that was found to be large was α, which was determined to be the order of unity. All other parameters were found to be small or nearly consistent with zero. The offset term δ was found to be nonzero in some cases. Since it was independent of the orientation of the polarizations of the PPT and the neutron beam, it must have originated in the proton beam. Attempts to identify a source for this effect have been unsuccessful.

A large number of systematic errors that might affect ϵ were considered. These included (1) the losses of beam between the SEM and LDT, which could be different for the two spin states because of possible beam width changes (see Fig. 8) or beam angle changes caused by the beam feedback system (see Fig. 9); (2) changes in the number of neutrons at the collimator exit due to beam width or angle changes with spin, and with the LDT shape and collimator acceptance; (3) changes in the fraction of beam missing the PPT related to (1) and (2) above; (4) slight differences in beam or PPT polarization magnitudes; (5) the effects of random coincidences with cosmic ray events and unequal normal and reverse beam intensities; (6) the effects of CASTOR and LORRAINE fringe fields on beam spin in different parts of the beam spot; and (7) errors in the definition of t due to slight differences in average timing from the two photomultipliers on a single counter. These differences would lead to offsets of the counter center signal from the center of the FTDC range. In essentially all cases, the estimated magnitude of the effect on $\Delta\sigma_L$ was much smaller than the error on $\Delta\sigma_L$, although there is some possibility that

TABLE II. Results from correlation fits to data. The "scheme" column indicates the method: i refers to the FTDC plane and $i\times j$ refers to COINC planes. With the exception of $\Delta\sigma_L$, only those parameters $\geq 3\sigma$ from zero were included in the fits. The quantity K_{eff} is the effective spin transfer, from Table I.

T_{lab} (MeV)	Scheme	$\Delta\sigma_L(K_{\text{eff}}/2A)$	1000α	1000β	1000γ	1000δ	$\sqrt{\chi^2/df}$
484[a]	1	−0.001 38±0.000 39					1.47
	2	−0.000 93±0.000 30	790±70				0.95
	1×2	−0.001 70±0.000 50					1.59
	2×3	−0.001 32±0.000 59	970±130				1.14
484[b]	1	−0.001 39±0.000 28		1.77±0.23			1.40
	2	−0.000 53±0.000 27		1.16±0.16			1.43
	1×2	−0.001 82±0.000 30		1.45±0.20			1.40
	2×3	−0.001 06±0.000 43		1.44±0.29			1.38
568[c]	1	−0.001 11±0.000 31	904±69				1.14
	2	−0.000 70±0.000 38	1193±99				1.25
	3	−0.000 91±0.000 35	1443±84				1.37
	1×2	−0.001 02±0.000 43	949±94				1.21
	2×3	−0.000 60±0.000 63	1364±141				1.14
	3×4	−0.000 93±0.000 61	1633±142				1.23
634[c]	1	−0.000 20±0.000 25	1183±80			−0.65±0.12	1.30
	2	−0.000 77±0.000 28	1245±92			−0.84±0.14	1.31
	3	−0.000 37±0.000 33	1501±107			−0.71±0.17	1.24
	1×2	−0.001 09±0.000 32	1107±104			−0.68±0.16	1.10
	2×3	−0.000 92±0.000 44	1185±145			−0.55±0.23	1.27
	3×4	−0.000 70±0.000 43	1134±138			−0.91±0.22	1.12
720[d]	1	−0.001 27±0.000 22			1420±480	+0.39±0.11	1.16
	2	−0.001 37±0.000 32					1.29
	1×2	−0.001 30±0.000 28			3640±530	+0.76±0.14	1.13
788[d]	1	−0.001 36±0.000 22		0.52±0.10			1.36
	2	−0.000 94±0.000 23				−0.55±0.12	1.28
	1×2	+0.000 25±0.000 30				−0.74±0.15	1.38
788[c]	1	−0.001 62±0.000 17				−0.71±0.08	1.28
	2	−0.001 16±0.000 20					1.21
	3	−0.000 72±0.000 31	939±99				1.64
	1×2	−0.001 66±0.000 22					1.44
	2×3	−0.001 60±0.000 31					1.13
	3×4	−0.001 92±0.000 31					1.21

[a]First running period.
[b]Detector moved, first running period.
[c]Second running period.
[d]Buncher was not monitored, first running period.

the quantity δ in Eq. (8) may be related to a beam angle or width change with spin [effects (1)–(3)]. In general, the large number of runs at each energy (50–100) with different PPT spin direction and CASTOR field direction canceled out most of these systematic effects.

Several tests of other systematics were also performed. For example, the measured asymmetry with the PPT unpolarized was consistent with zero, as expected. A nonzero effect would indicate either a systematic error or a parity violation. Another test involved combining the data from the first, third, fifth, etc. pairs of normal and reverse beam spin periods into "fake normal" counts and from the even pairs into "fake reverse" counts. The resulting asymmetries were computed and are expected to be consistent with zero if systematic errors are small. The observed fake asymmetries were consistent with zero in all cases. In addition, the *np* total cross section was measured at 568 (two runs) and 634 MeV (three runs) using a combination C/CH_2 target mounted vertically on a pneumatic piston, which was controlled electronically using the normal and reverse accelerator signals. The thickness of the CH_2 target was 1.4 cm and the thickness of the C target ($\approx$0.5 cm) was such that both targets had the same areal density of carbon. Although the statistics were poor, the cross sections derived from the measured normal and/or reverse asymmetries were approximately 44 ± 13 mb and 25 ± 7 mb for 568 and 634 MeV, respectively. These are consistent with the known [58–60] values of $\sigma(np)$ to within one or two standard deviations, respectively.

IV. RESULTS AND INTERPRETATION

The final results for $\Delta\sigma_L(np)$, which were found by taking a weighted average of the FTDC values in Table II, are given in Table III and plotted in Fig. 10 along with the data from other sources. The weights were taken from the statistical errors and increased by the square root of the reduced χ^2 shown in Table II to account for beam monitor (SEM) uncertainties. The normalization uncertainty for $\Delta\sigma_L(np)$ is estimated at 9.3% of its absolute value for the data of the first set of runs and at 10.8% for those of the second set. Table II indicates the distribution of the data between the run sets. The uncertainty in Table III includes contributions from the target constant (6.1% and 8.2%, for the respective sets), the polarizations of the proton beam (1%) and the PPT (6.2%), and the error due to having a target of finite size (1%), which was taken to correspond to one-half of the measured fraction of the beam missing the PPT. The uncertainty in the polarization of the neutron beam ($\approx$3%) is also included. However, this depends on the existing *np* analyzing-power data [38], which differ in the relevant kinematic regions by $\sim$10%, as described in Ref. [57]. Thus there is some chance that the systematic error on the neutron beam polarization is considerably underestimated. A 10% change in the K parameters will not change the values for $\Delta\sigma_L(np)$ by more than essentially one sigma of the statistical error.

The $\Delta\sigma_L(np)$ results are consistent with data measured at PSI [28] and Saclay [29,30], but are at variance

TABLE III. World $\Delta\sigma_L(np)$ data. The errors are given in the order statistical and systematic, respectively. The $\Delta\sigma_L(I{=}0)$ data are calculated from the *np* data using an interpolation of $\Delta\sigma_L(pp)$ values to subtract the $I{=}1$ part. In some cases, the existing data have been rounded to fewer significant digits than are given in the original references.

$T_{\rm lab}$ (MeV)	$\Delta\sigma_L(np)$ (mb)	$\Delta\sigma_L(I{=}0)$ (mb)	Reference
180	−31.1±9.4±2.0	−35.2±18.9±4.0	[28]
225	−26.6±3.4±1.6	−25.5±7.0±3.2	[28]
277	−22.0±2.7±1.2	−16.2±5.5±2.5	[28]
312	−21.7±5.9±0.31	−17.3±11.9±0.62	[30]
332	−17.9±1.8±0.95	−11.0±3.7±1.9	[28]
390	−14.8±1.0±0.82	−9.9±2.1±1.6	[28]
459	−9.1±0.8±0.60	−4.6±1.6±1.2	[28]
484	−6.07±1.14±0.56	−0.35±2.29±1.12	Present work
537	−7.9±0.6±0.54	−6.1±1.2±1.1	[28]
568	−5.26±1.35±0.57	−0.87±2.71±1.14	Present work
630	−4.95±1.12±0.48	+1.92±2.26±0.96	[30]
634	−2.23±1.09±0.24	+7.40±2.20±0.48	Present work
720	−6.60±1.10±0.61	+3.73±2.23±1.22	Present work
788	−6.65±0.64±0.67	+3.91±1.34±1.34	Present work
800	−9.51±1.04±0.52	−2.24±2.12±1.04	[30]
840	−9.89±0.72±0.40	−4.03±1.50±0.80	[30]
880	−9.8±1.5±0.36	−4.6±3.0±0.72	[30]
940	−9.35±0.60±0.33	−4.82±1.29±0.66	[30]
980	−9.2±2.6±0.55	−5.0±5.3±1.1	[30]
1000	−8.89±0.78±0.42	−4.80±1.62±0.84	[30]
1080	−4.9±2.3±0.35	+2.0±4.6±0.70	[30]
1100	−7.80±0.72±0.44	−3.95±1.50±0.88	[30]

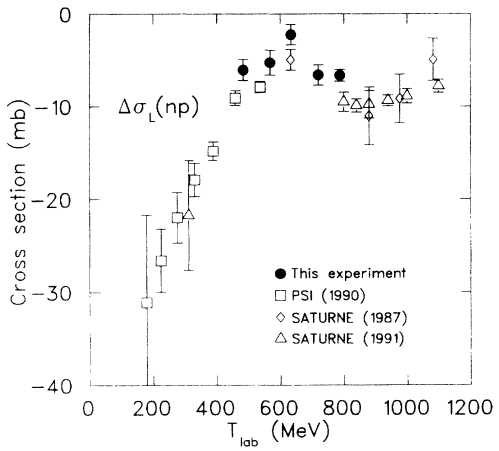

FIG. 10. World $\Delta\sigma_L(np)$ data as a function of incoming kinetic energy of the neutron beam in the laboratory frame, including the results of the present experiment, given with statistical errors only.

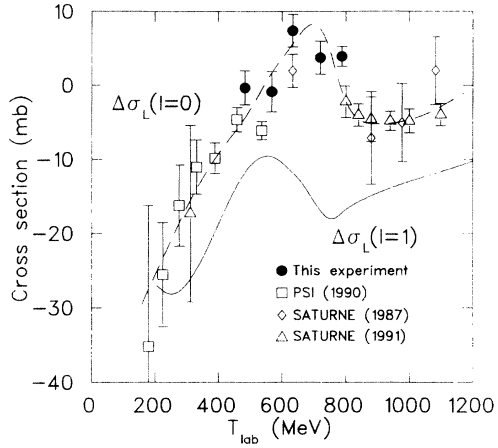

FIG. 12. Comparison of interpolated $\Delta\sigma_L(pp)$ (solid line) and $\Delta\sigma_L(I{=}0)$ (dashed line) data. The curve drawn through $I{=}0$ data is to guide the eye only. Note the similarity between $\Delta\sigma_L$ for both $I{=}0$ and $I{=}1$ channels.

with the Argonne $\Delta\sigma_L(np)$ data as derived from $\Delta\sigma_L(pd)$ [25]. The source of this discrepancy is not known, but it may be related to the forward $NN \rightarrow NN$ amplitudes used to obtain $\Delta\sigma_L(np)$ from the $\Delta\sigma_L(pd)$ measurements. A new dispersion relation analysis of these amplitudes is in progress [61], using all available $\Delta\sigma_L(np)$ and $\Delta\sigma_T(np)$ results. It is planned to calculate the pd total cross sections using these amplitudes, Glauber theory [62], and Fermi smearing corrections.

It is straightforward to extract $\Delta\sigma_L(I{=}0)$ cross sections from $\Delta\sigma_L(np)$ data by using the formula

$$\Delta\sigma_L(I{=}0) = 2\Delta\sigma_L(np) - \Delta\sigma_L(pp)\ . \qquad (10)$$

This has been done using the present data combined with the PSI and Saclay data. Values of $\Delta\sigma_L(pp)$ were found with an interpolation curve [15,63–65], shown in Fig. 11. The results for $\Delta\sigma_L(I{=}0)$ are given in Table III and shown in Fig. 12. Note that there is reasonable agreement among the three data sets, which were measured at different laboratories.

In comparing $\Delta\sigma_L(pp) = \Delta\sigma_L(I{=}1)$ and $\Delta\sigma_L(I{=}0)$, a striking similarity in the energy dependence is seen. Figure 12 shows both $\Delta\sigma_L(I{=}0)$ data and the interpolation curve for $\Delta\sigma_L(pp)$ data. Since the $I{=}0$ channel does not include πd or $N\Delta$ production, this similarity suggests that the structure in $\Delta\sigma_L(pp)$ may be related to some other process. Bystricky *et al.* [31] studied various NN inelastic cross sections and found that, in contrast to common prejudice, inelastic processes in the $I{=}0$ channel play an important role even below 600 MeV, so they cannot be neglected (see Fig. 13). They also observed, in general, that isosinglet cross sections are smaller than isotriplet ones, while the opposite is true for two-pion production processes in some energy regions. This allows for the possible existence of $I{=}0$ dibaryon resonances or inelastic threshold effects.

An attractive aspect of total cross-section data is that they are linear in the imaginary parts of the NN scatter-

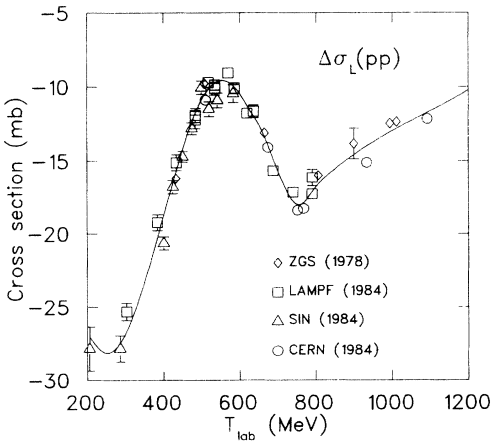

FIG. 11. Selected $\Delta\sigma_L(pp)$ data and interpolation curve used to extract the $I{=}0$ component from $\Delta\sigma_L(np)$.

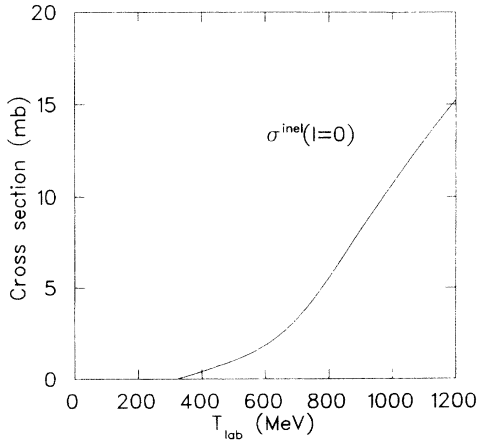

FIG. 13. Inelastic total cross section for $I{=}0$ NN scattering. The curve is calculated using parameters from a global fit to NN inelastic cross sections [31].

ing amplitudes, thereby providing valuable information concerning inelasticities. In addition, differences in total cross sections are free of large backgrounds. Expanding $\Delta\sigma_L$ in terms of partial waves,

$$\Delta\sigma_L = \frac{4\pi}{k^2}\mathrm{Im}\sum_J\Big[(2J+1)(R_J - R_{JJ}) + R_{J+1,J} - R_{J-1,J} - 4\sqrt{J(J+1)}\,R^J\Big], \quad (11)$$

while $\Delta\sigma_T$ and σ^{tot} in terms of partial waves are given by

$$\Delta\sigma_T = \frac{4\pi}{k^2}\mathrm{Im}\sum_J\Big[(2J+1)R_J - (J+1)R_{J+1,J} - JR_{J-1,J} + 2\sqrt{J(J+1)}\,R^J\Big] \quad (12)$$

and

$$\sigma^{\mathrm{tot}} = \frac{2\pi}{k^2}\mathrm{Im}\sum_J\big[(2J+1)(R_J + R_{J-1,J} + R_{J+1,J} + R_{JJ})\big], \quad (13)$$

where k is the c.m. wave number, J is the total angular momentum of the NN system, R_J represent singlet partial waves, R_{LJ} are triplet partial waves, and R^J are mixing amplitudes associated with the coupled triplets.

According to Eq. (11), the singlet R_J contributes positively (can give bumps) to $\Delta\sigma_L$, while the uncoupled-triplet R_{JJ} contributes negatively (can give dips) to $\Delta\sigma_L$. The contributions to $\Delta\sigma_L$ from the coupled triplets $R_{J\pm1,J}$ and R^J are more difficult to determine. From the behavior of the $\Delta\sigma_L(I{=}0)$ data, it is tempting to describe the observed structure as a bump centered at about 625 MeV. It therefore seems possible that the R_J might be the source of this bump. If contributions from other partial waves constitute a smooth background, this also suggests that a bump should be seen in $\sigma^{\mathrm{tot}}(I{=}0)$ as well, according to Eq. (13).

Values of this total cross section were derived from np and pp data and the relation $\sigma(I{=}0) = 2\sigma(np) - \sigma(pp)$. Using experimental values of $\sigma^{\mathrm{tot}}(pp)$ [66,67], a spline-fit routine was used to produce the curve through the pp data shown in Fig. 14. The np data in the energy range 200–1200 MeV are shown in Fig. 15. While the data of Grundies *et al.* [58] agree with those of Lisowski *et al.* [59], a systematic normalization difference with the data of Devlin *et al.* [60] is suggested in the region where they overlap. The resulting extracted $I{=}0$ total cross sections are shown in Fig. 16. A small change in slope at about 600 MeV is suggested here, which may be related to the rise of the inelastic cross section shown in Fig. 13.

According to the partial wave expansion for the cross-section observables [Eqs. (11) and (13)], the contribution of R_J to $\Delta\sigma_L$ and σ^{tot} is in the proportion 2:1, respectively. From Fig. 12, the structure in $\Delta\sigma_L(I{=}0)$ centered near 625 MeV could be viewed as a 6-mb bump. If it is due to R_J, structure at the 3-mb level might be seen in the total cross section near 625 MeV as well. Such structure is present in $\sigma^{\mathrm{tot}}(I{=}0)$ near 650 MeV (see Fig. 16). In the presence of a strongly energy-dependent back-

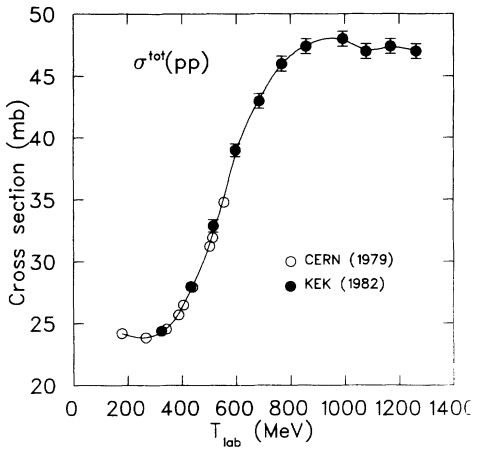

FIG. 14. Selected pp total cross-section data from Ref. [68] and an interpolation curve used for extracting the $I{=}0$ component from np total cross-section data.

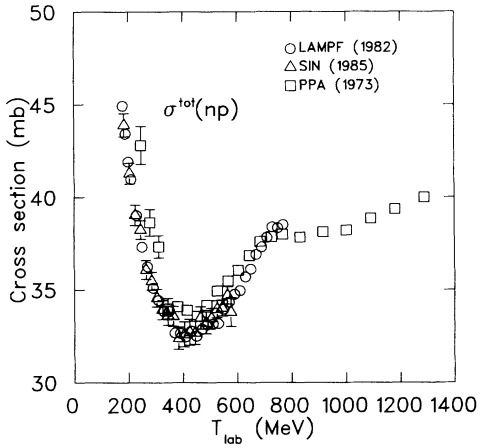

FIG. 15. Selected measured np total cross-section data from Ref. [68].

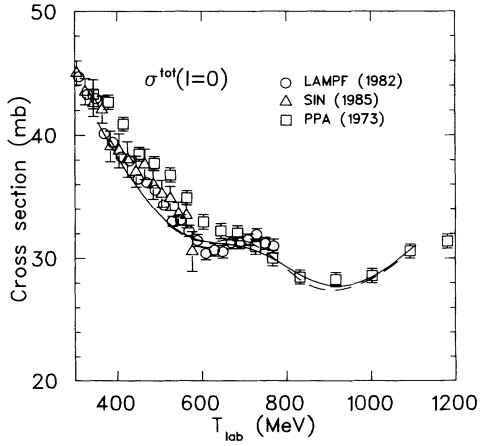

FIG. 16. The $I{=}0$ total cross section calculated using np data and interpolated pp data, together with Breit-Wigner fits. The singlet (solid line) and triplet (dashed line) curves are similar.

ground such a small shift in the position of a bump is possible.

A previous paper [33] reported results from fitting Breit-Wigner resonance curves to the $\Delta\sigma_L$ data. It is appropriate here to describe these fits in more detail. A partial wave with a resonance at c.m. energy E_R, with elastic width $\Gamma_{\rm el}$ and total width Γ, can be parametrized at c.m. energy E in terms of a Breit-Wigner formula

$$a = \frac{\Gamma_{\rm el}}{2(E_R - E) - i\Gamma} \approx \frac{\Gamma_{\rm el}}{\Gamma} \frac{\sqrt{\gamma}\,(m_R^2 - s) + i\gamma}{(m_R^2 - s)^2 + \gamma}\,, \qquad (14)$$

where $E_R + E \approx 2E_R$, $\sqrt{s} = 2E$, $m_R = 2E_R$, and $\gamma = 4m_R^2\Gamma^2$. For a singlet resonance ($R_J = a$),

$$\Delta\sigma_L^{\rm res} = \Delta\sigma_T^{\rm res} = 2\sigma_{\rm tot}^{\rm res} = \frac{4\pi}{k^2}(2J+1)\,{\rm Im}\,R_J = \frac{4\pi}{k^2}\frac{x\gamma}{(m_R^2 - s)^2 + \gamma}\,, \qquad (15)$$

with $x = (2J+1)\Gamma_{\rm el}/\Gamma$, which is sometimes referred to as the elasticity. The coupled-triplet partial waves were parametrized in terms of a mixing parameter ϵ_J in Ref. [26] as

$$\begin{pmatrix} R_{J-1,J} & R^J \\ R^J & R_{J+1,J} \end{pmatrix} = \frac{a}{1+\epsilon_J^2}\begin{pmatrix} 1 & \epsilon_J \\ \epsilon_J & \epsilon_J^2 \end{pmatrix}\,, \qquad (16)$$

and so, for coupled-triplet resonances,

$$\Delta\sigma_L^{\rm res} = \frac{4\pi}{k^2}\frac{\Gamma_{\rm el}}{\Gamma}\frac{\gamma}{(m_R^2 - s)^2 + \gamma} \times \frac{-1 + \epsilon_J^2 - 4\epsilon_J\sqrt{J(J+1)}}{1+\epsilon_J^2}\,,$$

$$\Delta\sigma_T^{\rm res} = \frac{4\pi}{k^2}\frac{\Gamma_{\rm el}}{\Gamma}\frac{\gamma}{(m_R^2 - s)^2 + \gamma} \times \frac{-J - (J+1)\epsilon_J^2 + 2\epsilon_J\sqrt{J(J+1)}}{1+\epsilon_J^2}\,,$$

$$\sigma_{\rm tot}^{\rm res} = \frac{2\pi}{k^2}\frac{x\gamma}{(m_R^2 - s)^2 + \gamma}\,. \qquad (17)$$

The database of the cross sections used in the Breit-Wigner fits of $\Delta\sigma_L$, $\Delta\sigma_T$, and $\sigma^{\rm tot}$ is given in Ref. [68]. A linear background was assumed for $\Delta\sigma_L$ and $\Delta\sigma_T$ and a quadratic one for $\sigma^{\rm tot}$. Fits were made over the region of $p_{\rm lab}$ from 0.8 to 1.8 GeV/c. The I=0 data used were extracted from cross-section data. When necessary, cubic splines were used to interpolate missing data For a singlet resonance, the best fit to the data from the three cross sections was obtained with $m_R = 2214 \pm 15$ (stat) ± 6 (syst) MeV, $\Gamma = 75 \pm 21 \pm 12$ MeV, and $x = (2J+1)\Gamma_{\rm el}/\Gamma = 1.01 \pm 0.15 \pm 0.15$. The systematic error includes a $\pm 10\%$ uncertainty in the neutron beam polarization for these new $\Delta\sigma_L$ data. For J=1, this resonance couples much more strongly to the elastic channel ($\Gamma_{\rm el}/\Gamma = 0.3$) than the I=1 dibaryons do, while for J=3, it couples about the same. The resonance parameters are fairly insensitive to the errors associated with the data.

Attempts were made for a fit of both J=1 and J=3 to a coupled-triplet resonance. For both values of J, ϵ_J came out close to $-\sqrt{(J+1)/J}$. The resonance contribution therefore is similar to the singlet case with $\Delta\sigma_L = 2\sigma^{\rm tot} = -\Delta\sigma_T$. The resonance parameters of this fit are $m_R = 2203$ MeV, $\Gamma = 34$ MeV, $x = 0.654$, and $\epsilon_J = -1.41$.

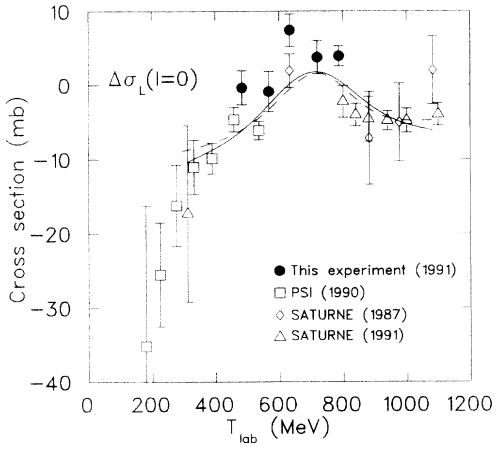

FIG. 17. Breit-Wigner fits to $\Delta\sigma_L(I{=}0)$ data. The singlet (solid line) and triplet (dashed line) curves are similar.

The difference between the two fits is hardly visible in $\sigma^{\rm tot}$ and $\Delta\sigma_L$ (see Figs. 16 and 17), but, for $\Delta\sigma_T$ (Fig. 18), the difference is obvious. In $\Delta\sigma_T$, this resonance appears as a bump of the same size as in $\Delta\sigma_L$, but positive for the singlet case and negative for the coupled-triplet case. The existing $\Delta\sigma_T$ data are consistent with either such a bump or dip. To clarify this situation, more measurements of $\Delta\sigma_T(np)$ are needed in the 1.2–1.5-GeV/c momentum region.

Recently, Hoshizaki *et al.* [10] published I=0 phase shift analyses that included the present data. They pointed out [69] that the peak position in $\Delta\sigma_L(I{=}0)$ coincided with a peak in the I=0 reaction cross section reported three decades ago by Dunaitsev and Prokoshkin

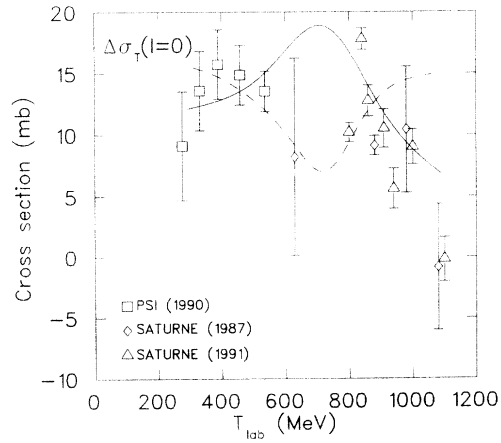

FIG. 18. Breit-Wigner fits to $\Delta\sigma_T(I{=}0)$ data, showing that the singlet partial wave (solid line) produces a bump and the coupled triplet partial wave (dashed line) gives a dip. The existing data are consistent with either curve.

[70], while, twenty years later, Dakhno *et al.* [71] did not find such a peak. They used the globally fitted total reaction *np* cross sections of the Saclay-Geneva group [31] in calculating their phase shifts. Two analyses were performed: one with no inelasticity and one with the inelasticity allowed to vary for the $^3S_1$, $^1P_1$, and $^3D_{1,2,3}$ states. They conclude that inelasticity in the I=0 channel is important above 600 MeV. Since the *np* database is incomplete, they did not insist on uniqueness of the solution. They also reported finding a resonance in the $^1P_1$ partial wave, and, after fitting with a Breit-Wigner curve, they obtained the resonance parameters m_R = 2168 MeV, Γ = 25 MeV, and Γ_{el}/Γ = 0.2. They also pointed out that measurements of $\Delta\sigma_T(np)$ are needed to confirm a predicted peak in the I=0 total reaction cross section.

V. SUMMARY

The quantity $\Delta\sigma_L(np)$, the difference between neutron-proton total cross sections for pure longitudinal spin states, has been measured at LAMPF for the five laboratory energies: 484, 568, 634, 720, and 788 MeV. The work was carried out as part of a program of measurements of *np* scattering aimed at determining the I=0 *NN* amplitudes at energies up to 800 MeV.

The I=0 *NN* amplitudes can be determined in a straightforward way from the measured *np* and *pp* data. The spin-averaged total cross section $\sigma^{tot}(np)$ together with $\Delta\sigma_L(np)$ directly measure the imaginary parts of two forward *np* amplitudes, while $\Delta\sigma_T(np)$ measures the imaginary part of a third amplitude.

Measurements of $\Delta\sigma_L(np)$ using a free neutron beam can be compared to values of $\Delta\sigma_L(pn)$ as derived from $\Delta\sigma_L(pd)$ data. Comparisons can check the validity of the corrections used in extracting the $\Delta\sigma_L(pn)$ results.

The experiment entailed the use of several separate specialized techniques: the generation of a polarized neutron beam, strict monitoring of the proton and neutron beam intensities and polarizations, the operation of a beam buncher and beam steering system, the operation of a polarized proton target, and a neutron counter array. The beam buncher and beam steering system were new additions to LAMPF and helped to reduce systematic effects due to the P^- beam.

The coincidence and FTDC logic used to obtain the positions of scattered particles were described, as well as the off line analysis of the data and estimates of the systematic errors. The results of the coincidence and FTDC methods were essentially consistent with each other. Systematic effects were reduced by frequent beam and polarized target spin direction reversals. In addition, data with the target empty and C/CH_2 target comparisons were used to study systematic effects. The estimated magnitude of the systematic effects on $\Delta\sigma_L$ is small.

The extraction of $\Delta\sigma_L(I$=0) from the $\Delta\sigma_L(np)$ data was described and compared to its I=1 counterpart, which has a similar energy dependence. It was argued that inelastic thresholds or resonances are not likely to be responsible for the structure in I=0 near 650 MeV. A Breit-Wigner fit, which included other cross-section data, was discussed. When combined with other data, the $\Delta\sigma_L$ data were found to contain structure consistent with a Breit-Wigner resonance in the singlet or coupled-triplet partial waves. As measurements of $\Delta\sigma_T(np)$ between 500 and 800 MeV are lacking, a determination of which partial wave is responsible for the structure, either a singlet or coupled triplet, is not possible without a phase-shift analysis.

ACKNOWLEDGMENTS

We would like to thank the polarized-target, mechanical, cryogenic, computing, electronics, and accelerator operations groups at LAMPF for their assistance throughout the experiment. In particular, we thank M. McNaughton and O. van Dyck for their assistance with beam tuning and the beam feedback steering system, J. Dawson (Argonne National Laboratory) for designing the FTDC's provided for the experiment, and T. Kasprzyk (also at Argonne) for help with the polarized target. This work was supported in part by the U.S. Department of Energy, Contract Nos. W31-109-ENG-38, DE-AS05-76ER-04449, and DE-AS04-76ER-03591, and Grant Nos. DE-FG05-88ER-40399 and DE-FG04-88ER-40403.

[1] M. Lacombe, B. Loiseau, J.-M. Richard, R. Vinh Mau, J. Cote, P. Pires, and R. de Tourreil, Phys. Rev. D **12**, 1495 (1975); Phys. Rev. C **21**, 861 (1980).

[2] R. Machleidt, K. Holinde, and Ch. Elster, Phys. Rep. **149**, 1 (1987); Ch. Elster, W. Ferchländer, K. Holinde, D. Schütte, and R. Machleidt, Phys. Rev. C **37**, 1647 (1988).

[3] M. Betz and T.-S. H. Lee, Phys. Rev. C **23**, 375 (1981); T.-S. H. Lee, Phys. Rev. Lett. **50**, 1571 (1983); Phys. Rev. C **29**, 195 (1984); T.-S. H. Lee and A. Matsuyama, *ibid.* **32**, 1986 (1985); **36**, 1459 (1987).

[4] R. Machleidt, in *Advances in Nuclear Physics*, edited by J. W. Negele and E. Vogt (Plenum, New York, 1989), Vol. 19, p. 189.

[5] I. Zahed and G. E. Brown, Phys. Rep. **142**, 1 (1986).

[6] U. G. Meissner and I. Zahed, in *Advances in Nuclear Physics*, edited by J. W. Negele and E. Vogt (Plenum, New York, 1986), Vol. 17, p. 143.

[7] C. W. Wong, Phys. Rep. **136**, 1 (1986).

[8] F. Myhrer and J. Wroldsen, Rev. Mod. Phys. **60**, 629 (1988).

[9] R. Vinh Mau, in *International Nuclear Physics Conference, São Paulo, Brazil, 1989*, edited by M. S. Hussein *et al.* (World Scientific, Singapore, 1990).

[10] Y. Higuchi, N. Hoshizaki, H. Masuda, and H. Nakao, Prog. Theor. Phys. **86**, 17 (1991); N. Hoshizaki and T. Watanabe, *ibid.* **86**, 321 (1991).

[11] R. A. Arndt, J. S. Hyslop, and L. D. Roper, Phys. Rev. D **35**, 128 (1987); R. A. Arndt, *ibid.* **37**, 3665 (1988).

[12] J. Bystricky, C. Lechanoine-Leluc, and F. Lehar, J. Phys. (Paris) **48**, 199 (1987); C. Lechanoine-Leluc, F. Lehar, P. Winternitz, and J. Bystricky, *ibid.* **48**, 985 (1982).

[13] D. V. Bugg, Phys. Rev. C **41**, 2708 (1990); R. Dubois, D. Axen, R. Keeler, M. Comyn, G. A. Ludgate, J. R. Richardson, N. M. Stewart, A. S. Clough, D. V. Bugg, and J. A. Edgington, Nucl. Phys. **A377**, 554 (1982).
[14] G. M. Shkylarevskii, Yad. Fiz. **47**, 117 (1988) [Sov. J. Nucl. Phys. **47**, 76 (1988)].
[15] I. P. Auer, E. Colton, D. Hill, K. Nield, B. Sandler, H. Spinka, Y. Watanabe, A. Yokosawa, and A. Beretvas, Phys. Lett. **67B**, 113 (1977); I. P. Auer, A. Beretvas, E. Colton, D. Hill, K. Nield, H. Spinka, D. Underwood, Y. Watanabe, and A. Yokosawa, *ibid.* **70B**, 475 (1977); I. P. Auer, E. Colton, H. Halpern, D. Hill, H. Spinka, G. Theodosiou, D. Underwood, Y. Watanabe, and A. Yokosawa, Phys. Rev. Lett. **41**, 345 (1978).
[16] M. P. Locher, M. E. Sainio, and A. Švarc, in *Advances in Nuclear Physics* (Ref. [6]), p. 47.
[17] M. Roos *et al.*, Phys. Lett. **111B**, 1 (1982); G. P. Yost *et al.*, Phys. Lett. B **205**, 1 (1988).
[18] R. L. Shypit *et al.*, Phys. Rev. Lett. **60**, 901 (1988); Phys. Rev. C **40**, 2203 (1989).
[19] M. G. Ryskin and I. I. Strakovsky, Phys. Rev. Lett. **61**, 2348 (1988).
[20] N. Hoshizaki *et al.*, in *Proceedings of the Workshop on the Experiments by KEK Polarized Proton and Electron Beams, KEK, Ibaraki, Japan, 1988*, edited by T. Hasegawa *et al.* (KEK, Ibaraki, Japan, 1989), p. 201; N. Hoshizaki, in *Proceedings of the Seventh International Symposium on High-Energy Spin Physics, Protvino, U.S.S.R., 1986*, edited by A. A. Antipova (Institute for High Energy Physics, Serpukhov, U.S.S.R., 1987), Vol. 1, p. 177.
[21] T.-S. H. Lee, Phys. Rev. C **40**, 2911 (1989).
[22] N. Hiroshige *et al.*, Mod. Phys. Lett. A **5**, 207 (1990).
[23] T. Ueda, J. Phys. (Paris) Colloq. **51**, C6-399 (1990).
[24] For a recent review of this work see *Proceedings of the International Conference on Spin Observables of Nuclear Probes, Telluride, Colorado, 1988* (Plenum, New York, 1988).
[25] I. P. Auer, W. R. Ditzler, D. Hill, H. Spinka, N. Tamura, G. Theodosiou, K. Toshioka, D. Underwood, R. Wagner, and A. Yokosawa, Phys. Rev. Lett. **18**, 1177 (1981).
[26] W. Grein, A. Koenig, and P. Kroll, Phys. Lett. **96B**, 176 (1980); W. Grein and P. Kroll, Nucl. Phys. **A377**, 505 (1982).
[27] D. Underwood (unpublished).
[28] R. Binz *et al.*, in *Proceedings of the Twelfth International Conference on Few Body Problems, Vancouver, British Columbia, 1989*, edited by H. W. Fearing [Nucl. Phys. **A508**, 267c (1990)].
[29] F. Lehar *et al.*, Phys. Lett. B **189**, 241 (1987); in *PANIC '87*, Proceedings of the Eleventh International Conference on Particles and Nuclei, Kyoto, Japan, edited by S. Homma *et al.* [Nucl. Phys. **A478**, 533c (1988)].
[30] J. M. Fontaine *et al.*, Nucl. Phys. **B358**, 297 (1991).
[31] J. Bystricky, P. La France, F. Lehar, F. Perrot, T. Siemiarczuk, and P. Winternitz, J. Phys. (Paris) **48**, 1901 (1987).
[32] T. Tsuboyama, N. Katayama, F. Sai, and S. S. Yamamoto, Nucl. Phys. **A486**, 669 (1988).
[33] M. Beddo *et al.*, Phys. Lett. B **258**, 24 (1991).
[34] M. Beddo, Ph.D. thesis, New Mexico State University, 1990; Los Alamos National Laboratory Report No. LA-11905-T, 1990 (unpublished).
[35] G. G. Ohlsen, Los Alamos National Laboratory Report No. LA-4451, 1970 (unpublished).
[36] C. W. Bjork, Ph.D. thesis, University of Texas at Austin, 1975; Los Alamos National Laboratory Report No. LA-6192-T, 1976 (unpublished).
[37] P. J. Riley *et al.*, Phys. Lett. **103B**, 313 (1981).
[38] J. S. Chalmers *et al.*, Phys. Lett. **153B**, 235 (1985).
[39] H. M. Spinka, Argonne National Laboratory Report No. ANL-HEP-TR-88-14, 1988 (unpublished).
[40] Charge Pump Digitizer, Model No. RN-8111, Red Nun Instrument Corp., Westfield, NJ.
[41] E. P. Chamberlin, R. L. York, H. E. Williams, and E. L. Rios, in *Proceedings of the Fifth International Symposium on Polarization Phenomena in Nuclear Physics, Santa Fe, 1980*, AIP Conf. Proc. No. 69, edited by G. G. Ohlsen *et al.* (AIP, New York, 1981), p. 887.
[42] M. W. McNaughton, Los Alamos National Laboratory Report No. LA-8307-MS, 1980 (unpublished).
[43] M. W. McNaughton and E. P. Chamberlin, Phys. Rev. C **24**, 1778 (1981).
[44] Multichannel Analyzer for Charge, Voltage, or Time, Model No. 3001, Lecroy Research Systems, Spring Valley, NY.
[45] M. McNaughton, Los Alamos National Laboratory Progress Report No. LA-11339-PR, 1987 (unpublished).
[46] A. Abragam and M. Goldman, *Nuclear Magnetism: Order and Disorder* (Clarendon, Oxford, 1982); Rep. Prog. Phys. **41**, 395 (1978).
[47] M. Krumpolc and J. Roček, J. Am. Chem. Soc. **101**, 3206 (1979).
[48] Manufactured by Wang NMR, Inc., Livermore, CA 94550.
[49] D. Hill and T. Kasprzyk, Argonne National Laboratory Report No. ANL-HEP-PR-84-32, 1984 (unpublished).
[50] Optical coupling compound 22-3067, Dow Corning Corp., Midland, MI 48686.
[51] R. Garnett *et al.*, Nucl. Instrum. Methods **A309**, 508 (1991).
[52] Designed by J. Dawson, Argonne National Laboratory.
[53] W. C. Sailor, R. C. Byrd, and Y. Yariv, Nucl. Instrum. Methods **A277**, 599 (1989); Los Alamos National Laboratory Report No. LA-11348-MS, 1988 (unpublished).
[54] L. R. Biswell and R. E. Rajala, Los Alamos National Laboratory Report No. LA-4916-MS, 1972 (unpublished). Manufactured by BiRa Systems, Inc., Albuquerque, NM 87107.
[55] A. G. Worthing and J. Geffner, *Treatment of Experimental Data* (Wiley, New York, 1943), pp. 170–1 and 319.
[56] M. W. McNaughton *et al.*, Phys. Rev. C **44**, 2267 (1991); **45**, 2564 (1992); **48**, 256 (1993); M. W. McNaughton (private communication).
[57] V. Carlson *et al.* (unpublished).
[58] V. Grundies *et al.*, Phys. Lett. **158B**, 15 (1985).
[59] P. W. Lisowski *et al.*, Phys. Rev. Lett. **49**, 255 (1982).
[60] T. J. Devlin *et al.*, Phys. Rev. D **8**, 136 (1973).
[61] P. Kroll and P. Toumpas (unpublished).
[62] C. Sorensen, Phys. Rev. D **19**, 1444 (1979); G. Alberi, M. Bleszynski, T. Jaroszewicz, and S. Santos, *ibid.* **20**, 2437 (1979); W. Grein and P. Kroll, Nucl. Phys. **B157**, 529 (1979).
[63] I. P. Auer *et al.*, Phys. Rev. D **29**, 2435 (1984).
[64] E. Aprile-Giboni *et al.*, Nucl. Phys. **A431**, 637 (1984).
[65] J. Bystricky *et al.*, Phys. Lett. **142B**, 130 (1984).
[66] P. Schwaller *et al.*, Nucl. Phys. **A316**, 317 (1979).
[67] F. Shimizu *et al.*, Nucl. Phys. **A386**, 571 (1982).

[68] $\Delta\sigma_L$: present data supplemented by those of Ref. [29] (pn); Ref. [64] (pp); R. Binz *et al.* (unpublished) (np). $\Delta\sigma_T$: F. Perrot *et al.*, Nucl. Phys. **B278**, 881 (1986) (pp); F. Lehar *et al.*, Phys. Lett. B **189**, 241 (1987) (pn); and R. Binz *et al.* (unpublished) (np). $\sigma^{\rm tot}$: Refs. [66,67] (pp); Refs. [58,59] (np).

[69] N. Hoshizaki and T. Watanabe, Prog. Theor. Phys. **86**, 327 (1991).

[70] A. F. Dunaitsev and Yu. D. Prokoshkin, Zh. Eksp. Teor. Fiz. **38**, 747 (1960) [Sov. Phys. JETP **11**, 540 (1960)].

[71] L. G. Dakhno *et al.*, Leningrad Nuclear Physics Institute Report No. 692, 1981 (unpublished).